BSc thesis APPLIED MATHEMATICS & APPLIED PHYSICS

"Synchronisation along quantum trajectories of three coupled VdP oscillators"

TIM KLIJNJAN

Delft University of Technology

Supervisors

Dr. J.L.A Dubbeldam

Prof.Dr. Y.M. Blanter

Other committee members

Dr. R.C. Kraaij

Dr. M. Blaauboer

January, 2021

Delft

Abstract

Synchronisation is the remarkable phenomenon of in-phase movement of coupled oscillators during a prolonged period of time, which even occurs when these have different natural frequencies. This property is used in many fields like physics, biology and chemistry, to model various system behaviours, for instance: circadian rhythms in the chemistry of the eyes [1].
This thesis focuses on synchronisation and entanglement in systems consisting of quantum Van der Pol oscillators. After looking at the exemplary properties of the classical VdP oscillator, it follows the methods of [2] to explore the behaviour of two coupled QVdPOs, quantum Van der Pol oscillators, using Monte Carlo simulations for trajectories of this system. The system is then expanded to three-oscillator systems with all-to-all and chain coupling. The validity of the extension of the properties found in two QVdPOs in [2] with regard to synchronisation and entanglement is tested. Does an Arnold tongue, the region of parameters for which a system shows synchronisation, still exist and if so has its shape changed? Do synchronisation and strong entanglement still show a positive correlation?
Simulations of the 2-oscillator system gave results which were just slightly different from those obtained in[2], validating the occurrence of synchronisation within the Arnold tongue and showing a positive correlation between synchronisation and entanglement of the system. Both the 3-oscillator systems showed synchronisation as well in their respective Arnold tongues, which were increasingly smaller for the all-to-all coupled and the chain coupled system when compared to the 2-oscillator system. Overall, the amount of synchronisation, shown in three oscillators was very close to the amount shown in two oscillators when strongly coupled and just a little less for weak coupling. The correlation between synchronisation and strong entanglement was also found for three oscillators, though for weaker coupling the chain coupled system showed a little more entanglement than before.

Contents

1 Introduction

Synchronisation is a phenomenon seen in many quite different systems. The tendency of certain oscillators to move in-phase with one another when weakly coupled, is used in a plethora of fields within physics, biology and chemistry to predict how systems behave [3, 4]. For example, in [1] circadian rhythms in the chemistry of the eyes are modelled using three Van der Pol oscillators and their ability to synchronise.
In quantum mechanics synchronisation is also a widely researched topic [2, 5–9] since the understanding of the way oscillators behave can often provide very useful insights into how smaller systems, like salt crystals or hydrogen atoms, behave.
In this thesis we build upon the research done in [2]. There constraints to allow synchronisation in a system of two quantum Van der Pol oscillators, QVdPOs, and the relation of synchronisation and entanglement in the system were explored. Using their methods we first look at the same system to verify the results before expanding to a three-oscillator system. For the three oscillators, we look at all-to-all and chain coupling, for which in the end we provide an answer to whether or not the 3-oscillator systems show the same behaviour as the 2 oscillators with respect to synchronisation and entanglement.

To this end we first present a theoretical background in chapter 2. There properties of various systems with classical Van der Pol oscillators, CVdPOs, are explored, such as limit cycles and synchronisation. Regimes called Arnold tongues are found, in which synchronisation is possible, and these serve as a prediction for the quantum Arnold tongues. Lindblad master equations and stochastic Schrödinger equations are used to describe the quantum systems, followed by an introduction to the indicators we use to characterise their behaviour. In chapter 3 the results of the Monte Carlo simulations of the quantum systems are presented and connections between the various systems are made. From these results, we draw conclusions in chapter 4 and discuss the methods used, before suggesting some options for further research.

2 Theoretical background

2.1 One classical VdP oscillator

We first look at a system of one classical Van der Pol oscillator, as its behaviour is in many ways similar to the more complex systems probed later on. This CVdP oscillator is described by the non-linear Ordinary differential equation:

$$\ddot{x} + \mu(x^2 - 1)\dot{x} + \omega^2 x = 0 \tag{2.1}$$

Where x gives the perturbation from the equilibrium at $x = 0$, μ indicates the strength of the non-linear damping, which for $|x| < 1$ acts as a pumping term and ω is the eigenfrequency of the oscillator.

2.1.1 Stability of the CVdP oscillator

To find the parameters that lead to stable solutions 2.1 is rewritten as a system of two first order ODEs:

$$\begin{aligned} \dot{x} &= y \\ \dot{y} &= \mu(1 - x^2)y - \omega^2 x \end{aligned} \tag{2.2}$$

Or using matrix notation:

$$\dot{\mathbf{x}} = A\mathbf{x} + \mathbf{g}(\mathbf{x}) \tag{2.3}$$

With $\mathbf{x} = \begin{bmatrix} x \\ y \end{bmatrix}$, $A = \begin{bmatrix} 0 & 1 \\ -\omega^2 & \mu \end{bmatrix}$ and $\mathbf{g}(\mathbf{x}) = \begin{bmatrix} 0 \\ -\mu x^2 y \end{bmatrix}$

Since $\mathbf{g}(\mathbf{x})/\|\mathbf{x}\|$ vanishes for $\mathbf{x} = 0$ the eigenvalues of A can be calculated to determine stability [10]:

$$\begin{vmatrix} -\lambda & 1 \\ -\omega^2 & \mu - \lambda \end{vmatrix} = \lambda^2 - \lambda\mu + \omega^2 = 0 \tag{2.4}$$

Giving $\lambda = \frac{1}{2}\mu \pm \frac{1}{2}\sqrt{\mu^2 - 4\omega^2}$. The right part of which is imaginary when $|\mu| < 2|\omega|$ thus giving asymptotic stability for $\mu < 0$. The other case gives asymptotic stability within the same region of μ values since then $\sqrt{\mu^2 - 4\omega^2} \leq |\mu|$. Therefore the origin is a stable equilibrium solution for $\mu < 0$. How the oscillator moves towards the equilibrium can be illustrated using phase diagrams:

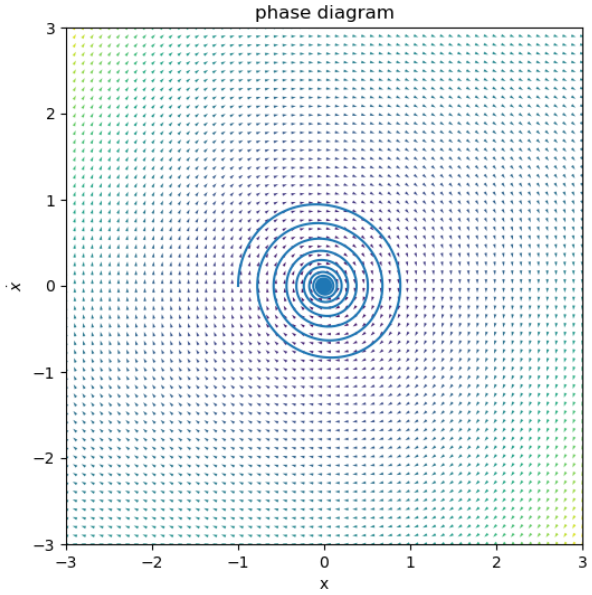

Fig. 2.1: Phase plot of one classical VdP, $\mu = -0.1, \omega = 1, x_0 = -1, \dot{x}_0 = 0, t_0 = 0, t_e = 5000$.

As shown in fig. 2.1, with partially imaginary eigenvalues, the system spirals down into the stable solution.

When μ is set to zero the system simplifies to:

$$\ddot{x} + \omega^2 x = 0 \tag{2.5}$$

Which is just the harmonic oscillator with solutions $x(t) = A\cos(\omega t + \phi)$. With the initial conditions determining the radius in phase space, this looks something like:

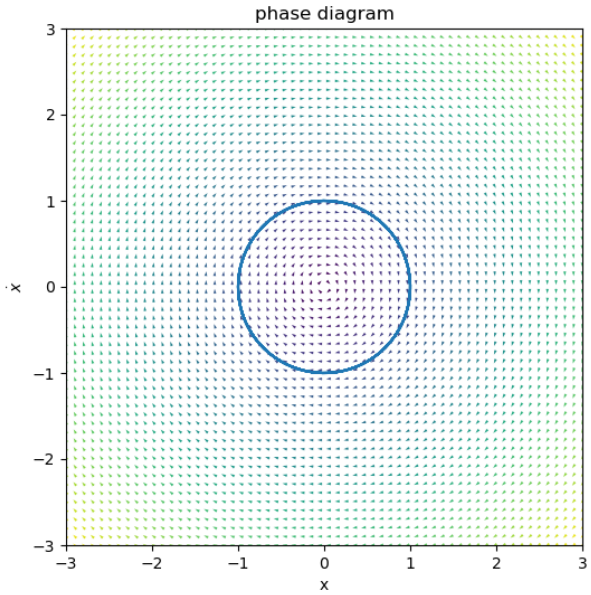

Fig. 2.2: Phase plot of the harmonic oscillator, $\mu = 0, \omega = 1, x_0 = -1, \dot{x}_0 = 0, t_0 = 0, t_e = 5000$.

2.1.2 Limit cycle of the CVdP oscillator

It remains to look at the case of $\mu > 0$, which according to the previous stability analysis, gives instability of the origin. However under this condition the system approaches a limit cycle, a closed trajectory in phase space, to which in this case all initial conditions, except the origin, converge. Existence and uniqueness of this LC are proven using Liénard's theorem [4]:
Liénard's equation: $\ddot{x} + f(x)\dot{x} + g(x) = 0$

Theorem 1 (Liénard's theorem)**.** *If $f(x)$ and $g(x)$ satisfy:*

1. *$f(x)$ and $g(x)$ are continuously differentiable for all x;*
2. *$g(-x) = -g(x)$ for all x;*
3. *$g(x) > 0$ for $x > 0$;*
4. *$f(-x) = f(x)$ for all x;*
5. *$F(x) = \int_0^x f(u)du$ has exactly one positive zero at $x = a$, is negative for $0 < x < a$, is positive and nondecreasing for $x > a$, and $F(x) \to \infty$ as $x \to \infty$*

Then Liénard's equation has a unique, stable limit cycle around the origin of its phase plane.

For the VdP oscillator we have $f(x) = \mu(x^2 - 1)$ and $g(x) = \omega^2 x$ in Liénard's equation, thus for positive values of μ Liénard's theorem gives the existence of a unique, stable limit cycle around the origin. For $\mu \ll 1$ and $\mu \to \infty$, the weakly and strongly non-linear regime respectively, the amplitude of this limit cycle is close to 2 and for the transitional area between those, formulas exist to approximate the amplitude [11]. Between those two regimes, the limit cycle takes on the shape shown in fig. 2.3(b), whereas μ increases the extrema deviate further from $\dot{x} = 0$.

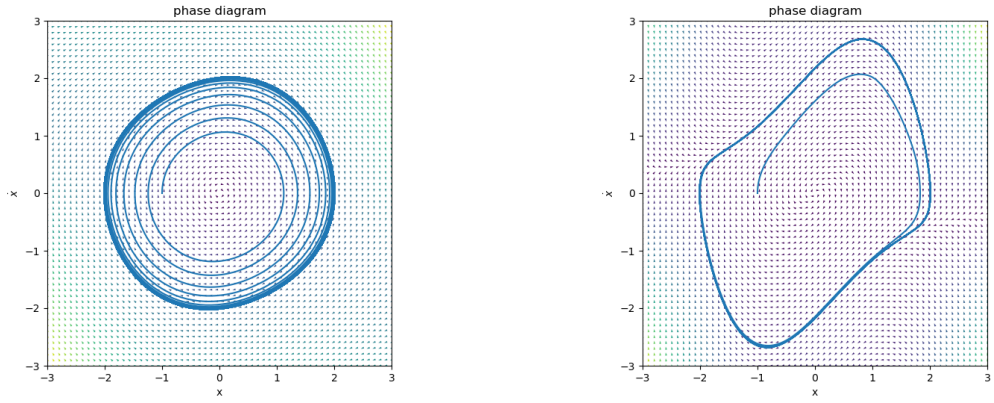

(a) **(b)**

Fig. 2.3: Limit cycle of the VdP oscillator in the (weakly) non-linear regime, $\omega = 1, x_0 = -1, \dot{x}_0 = 0$ (a): $\mu = 0.1$, (b): $\mu = 1$.

2.2 Two coupled CVdP oscillators

Proceeding from the single CVdP we now couple two oscillators. Since the oscillations of the coupled CVdPs are mainly of concern to describe dynamical systems, first of all conditions for the existence of the LC are explored.

2.2.1 LC of the coupled CVdP system

A system of coupled VdP oscillators is given by:

$$\begin{aligned} \ddot{x}_1 + \mu_1(x_1^2 - 1)\dot{x}_1 + \omega_1^2 x_1 + \sigma(x_2 - x_1) &= 0 \\ \ddot{x}_2 + \mu_2(x_2^2 - 1)\dot{x}_2 + \omega_2^2 x_2 + \sigma(x_1 - x_2) &= 0 \end{aligned} \tag{2.6}$$

Where the indices number the oscillators and σ is the strength of the coupling. To find which values for the various parameters lead to a limit cycle it, is useful to look at Hopf bifurcations of the system. A Hopf bifurcation is transitional point between the system having a stable equilibrium solution and having a stable LC. In order to find the Hopf bifurcation 2.6 can be written as a system of 4 first order ODE's:

$$\begin{aligned} \dot{x}_1 &= y_1 \\ \dot{y}_1 &= \mu_1(1 - x_1^2)\dot{x}_1 - \omega_1^2 x_1 - \sigma(x_2 - x_1) \\ \dot{x}_2 &= y_2 \\ \dot{y}_2 &= \mu_2(1 - x_2^2)\dot{x}_2 - \omega_2^2 x_2 - \sigma(x_1 - x_2) \end{aligned} \tag{2.7}$$

Which can be written using matrix notation as:

$$\dot{\mathbf{x}} = A\mathbf{x} + \mathbf{g}(\mathbf{x}) \tag{2.8}$$

With $\mathbf{x} = \begin{bmatrix} x_1 \\ y_1 \\ x_2 \\ y_2 \end{bmatrix}$, $A = \begin{bmatrix} 0 & 1 & 0 & 0 \\ \sigma - \omega_1^2 & \mu_1 & -\sigma & 0 \\ 0 & 0 & 0 & 1 \\ -\sigma & 0 & \sigma - \omega_2^2 & \mu_2 \end{bmatrix}$ and $\mathbf{g}(\mathbf{x}) = \begin{bmatrix} 0 \\ -\mu_1 x_1^2 y_1 \\ 0 \\ -\mu_2 x_2^2 y_2 \end{bmatrix}$

The characteristic polynomial of A can be found as:

$$\begin{aligned} P(\lambda) = \quad & \lambda^4 - (\mu_1+\mu_2)\lambda^3 + (\mu_1\mu_2 - 2\sigma + \omega_1^2 + \omega_2^2)\lambda^2 \\ & +(\mu_1\sigma - \mu_1\omega_2^2 - \mu_2\omega_1^2 + \mu_2\sigma)\lambda - \sigma(\omega_1^2+\omega_2^2) + \omega_1^2\omega_2^2 \end{aligned} \tag{2.9}$$

For a Hopf bifurcation we have one eigenvalue pair $\lambda = \pm i\omega$ for some $\omega \in \mathbb{R}$. Using this and the characteristic polynomial gives:

$$\begin{aligned} P(i\omega) = \quad & \omega^4 + (\mu_1+\mu_2)i\omega^3 - (\mu_1\mu_2 - 2\sigma + \omega_1^2 + \omega_2^2)\omega^2 \\ & +(\mu_1\sigma - \mu_1\omega_2^2 - \mu_2\omega_1^2 + \mu_2\sigma)i\omega - \sigma(\omega_1^2+\omega_2^2) + \omega_1^2\omega_2^2 \end{aligned} \tag{2.10}$$

The equation can be split into a real and an imaginary part, both of which must equal zero for $i\omega$ to be an eigenvalue:

$$\begin{aligned} \omega^4 - (\mu_1\mu_2 - 2\sigma + \omega_1^2 + \omega_2^2)\omega^2 - \sigma(\omega_1^2+\omega_2^2) + \omega_1^2\omega_2^2 &= 0 \\ (\mu_1+\mu_2)\omega^3 + (\mu_1\sigma - \mu_1\omega_2^2 - \mu_2\omega_1^2 + \mu_2\sigma)\omega &= 0 \end{aligned} \tag{2.11}$$

Solving the last equation gives $\omega = 0$ or $\omega^2 = -\frac{\mu_1\sigma - \mu_1\omega_2^2 - \mu_2\omega_1^2 + \mu_2\sigma}{\mu_1+\mu_2}$. Plugging the non-trivial solution into the first equation gives an implicit curve that describes where a Hopf bifurcation occurs:

$$\frac{(\mu_1\sigma - \mu_1\omega_2^2 - \mu_2\omega_1^2 + \mu_2\sigma)^2}{(\mu_1+\mu_2)^2} + \frac{(\mu_1\sigma - \mu_1\omega_2^2 - \mu_2\omega_1^2 + \mu_2\sigma)(\mu_1\mu_2 - 2\sigma + \omega_1^2 + \omega_2^2)}{\mu_1+\mu_2} - \sigma(\omega_1^2+\omega_2^2) + \omega_1^2\omega_2^2 = 0 \tag{2.12}$$

Where we require that $\mu_1 + \mu_2 \neq 0$ and $\frac{\mu_1\sigma - \mu_1\omega_2^2 - \mu_2\omega_1^2 + \mu_2\sigma}{\mu_1+\mu_2} < 0$, since $\mu_1 + \mu_2 = 0$ would only allow $\omega = 0$ and ω needs to be a real valued solution to the last equation of 2.11.
Using the description obtained above, we now look at a few cases for the coupled VdP system. First we assume no coupling between the oscillators, $\sigma = 0$, and equal eigenfrequencies, $\omega_1^2 = \omega_2^2 = \omega^2$. Combining these values with 2.12 gives: $\mu_1\mu_2 = 0$ ($\omega = 0$ is not accepted). Thus a Hopf bifurcation occurs when $\mu_1 = 0$ or $\mu_2 = 0$, analogous to the criterion for the existance of a LC for a single oscillator.

When the oscillators are coupled with strength σ, we obtain $\mu_1\mu_2 = \frac{\sigma^2}{\sigma - \omega^2} < 0$, since the second requirement gives $\sigma < \omega^2$. Therefore a positive value for μ_1 would give a negative value for μ_2 and vice versa:

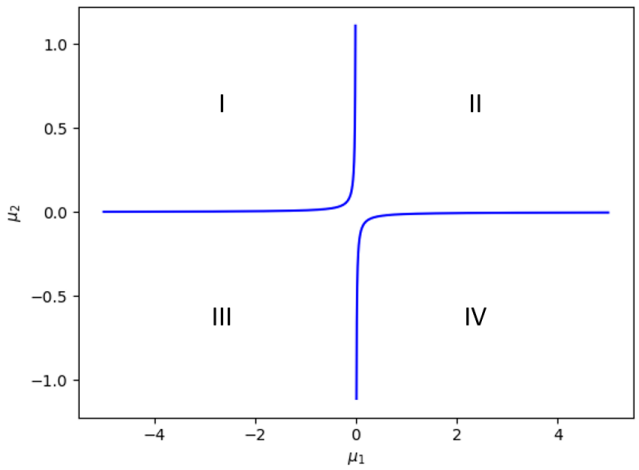

Fig. 2.4: Curve of μ-values for which a Hopf bifurcation occurs, $\sigma = 0.1, \omega_1^2 = \omega_2^2 = 1$

As μ_1 approaches plus or minus infinity μ_2 goes to zero. This makes sense because as the μ value of an oscillator goes to infinity, its amplitude becomes constant. In turn the other oscillator then practically is decoupled and experiences a constant driving force as well as a frequency shift, making stability dependent on only the μ of the oscillator itself.

Within the numbered areas in fig. 2.4, separated by the Hopf curve, the system shows different behaviour. In area **I** oscillator 1 has a stable equilibrium but is forced to circle around this due to the coupling to the stable limit cycle of oscillator 2. By adding energy to oscillator 1, oscillator 2 creates a limit cycle for the combined system. Similar behaviour is achieved in area **IV**, where the roles of both oscillators are flipped. For values inside area **II** both oscillators have a stable limit cycle, in area **III** however, both oscillators have the same equilibrium and the system collapses to zero displacement in combination with zero movement.

2.2.2 Synchronisation of two coupled CVdPOs

When multiple oscillators are connected through some kind of coupling, a phenomenon called synchronisation may occur. Synchronisation is achieved when the phase difference between two oscillators becomes constant for a prolonged period of time, which can even take place for oscillators with different natural frequencies. Conditions required for synchronisation can be attained from the system in complex amplitude form [3][8]:

$$\begin{aligned} \dot{\alpha}_1 &= -i\omega_1\alpha_1 + \tfrac{\gamma_1^{(1)}}{2}\alpha_1 - \gamma_2^{(1)}|\alpha_1|^2\alpha_1 + \left(\tfrac{D}{2} + iR\right)(\alpha_2 - \alpha_1) \\ \dot{\alpha}_2 &= -i\omega_2\alpha_2 + \tfrac{\gamma_1^{(2)}}{2}\alpha_2 - \gamma_2^{(2)}|\alpha_2|^2\alpha_2 + \left(\tfrac{D}{2} + iR\right)(\alpha_1 - \alpha_2) \end{aligned} \tag{2.13}$$

$\gamma_1^{(i)}$ and $\gamma_2^{(i)}$ are the negative and non-linear damping for oscillator i, $D \geq 0$ and $R \geq 0$ give the dissipative (non-conservative with energy loss to the environment) and reactive (conservative) coupling respectively. When uncoupled the oscillators have a stable limit cycle with amplitude $|\alpha_1| = \bar{r_i} = \sqrt{\gamma_1^{(i)}/2\gamma_2^{(i)}}$[7]. The system above can be written in terms of modulus and phase using $\alpha_i = r_i e^{i\phi_i}$:

$$\begin{aligned} \dot{r}_1 &= \left(\tfrac{\gamma_1^{(1)}}{2} - \gamma_2^{(1)} r_1^2\right) r_1 + \tfrac{D}{2}(r_2\cos(\theta) - r_1) - Rr_2\sin(\theta) \\ \dot{r}_2 &= \left(\tfrac{\gamma_1^{(2)}}{2} - \gamma_2^{(2)} r_2^2\right) r_2 + \tfrac{D}{2}(r_1\cos(\theta) - r_2) - Rr_1\sin(-\theta) \\ \dot{\theta} &= -(\omega_2 - \omega_1) + R\left(\tfrac{r_1}{r_2} - \tfrac{r_2}{r_1}\right)\cos(\theta) - \tfrac{D}{2}\left(\tfrac{r_1}{r_2} + \tfrac{r_2}{r_1}\right)\sin(\theta) \end{aligned} \tag{2.14}$$

Where $\theta = \phi_2 - \phi_1$. To see how these systems are equivalent, we substitute the modulus amplitude expression into 2.13 and divide by $e^{i\phi_i}$ giving for the left hand side $\dot{r}_i + i\dot{\phi}_i r_i$. Separating the real and imaginary parts of the obtained equations then gives:

$$\begin{aligned} \dot{r}_1 &= \left(\tfrac{\gamma_1^{(1)}}{2} - \gamma_2^{(1)} r_1^2\right) r_1 + \tfrac{D}{2}(r_2\Re\{e^{i\theta}\} - r_1) - Rr_2\Im\{e^{i\theta}\} \\ \dot{r}_2 &= \left(\tfrac{\gamma_1^{(2)}}{2} - \gamma_2^{(2)} r_2^2\right) r_2 + \tfrac{D}{2}(r_1\Re\{e^{-i\theta}\} - r_2) - Rr_1\Im\{e^{-i\theta}\} \\ \dot{\phi}_1 r_1 &= -\omega_1 r_1 + \tfrac{D}{2} r_2\Im\{e^{i\theta}\} + R(r_2\Re\{e^{i\theta}\} - r_1) \\ \dot{\phi}_1 r_2 &= -\omega_2 r_2 + \tfrac{D}{2} r_1\Im\{e^{-i\theta}\} + R(r_1\Re\{e^{-i\theta}\} - r_2) \end{aligned} \tag{2.15}$$

Substituting Euler's formula and subtracting the third equality form the last after division by r_i gives the previous system 2.14. Now focussing on a system with dissipative coupling only, we set $R = 0$. Assuming small coupling the dynamics of $\dot{r}_1$ and $\dot{r}_2$ can be neglected [8]. This gives the Adler equation for the relative phase [12]:

$$\dot{\theta} = -\Delta - \frac{DA}{2}\sin(\theta) \tag{2.16}$$

In this $\Delta = \omega_2 - \omega_1$ and $A = \bar{r}_1/\bar{r}_2 + \bar{r}_2/\bar{r}_1$. The steady-state solution is found by setting $\dot{\theta} = 0$ and can only exist when:

$$\left|\frac{2\Delta}{DA}\right| \leq 1 \tag{2.17}$$

Which for the coupling strength requires:

$$\frac{2|\Delta|}{A} \leq D \tag{2.18}$$

When the oscillators have equal damping rates ($\gamma_1^{(1)} = \gamma_1^{(2)}, \gamma_2^{(1)} = \gamma_2^{(2)}$), this results in $|\Delta| \leq D = \frac{V}{2}$ (where D can remain small when Δ is a small fraction of the natural frequencies), the classical Arnold tongue [2]:

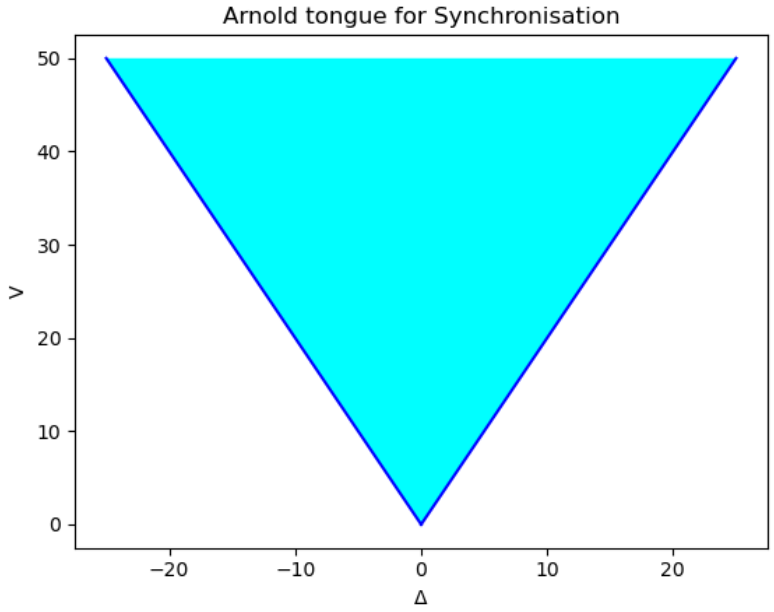

Fig. 2.5: Plot of the (blue) area in which conditions for synchronisation of two VdP oscillators with equal damping rates are met, also called the Arnold tongue. $V = 2D$.

2.3 Three coupled CVdP oscillators

Here two differently coupled systems of three classical Van der Pol oscillators will be presented, one of which has all-to-all coupling and the other has chain coupling. In the all-to-all coupled system energy can be transferred from each oscillator to one of the others in a fully symmetrical way. The chain coupling sees oscillators only linked to its two (or one for endpoints) direct neighbours.

2.3.1 Synchronisation of three all-to-all coupled CVdPOs

The Arnold tongue for three oscillators is found analogously to that for two oscillators, but the assumption of equal damping and pumping rates and $R = 0$ are made right away:

$$\begin{aligned} \dot{\alpha}_1 &= -i\omega_1\alpha_1 + \tfrac{\gamma_1^{(1)}}{2}\alpha_1 - \gamma_2^{(1)}|\alpha_1|^2\alpha_1 + \tfrac{D}{2}(\alpha_3 + \alpha_2 - 2\alpha_1) \\ \dot{\alpha}_2 &= -i\omega_2\alpha_2 + \tfrac{\gamma_1^{(2)}}{2}\alpha_2 - \gamma_2^{(2)}|\alpha_2|^2\alpha_2 + \tfrac{D}{2}(\alpha_3 + \alpha_1 - 2\alpha_2) \\ \dot{\alpha}_3 &= -i\omega_3\alpha_3 + \tfrac{\gamma_1^{(3)}}{2}\alpha_3 - \gamma_2^{(3)}|\alpha_3|^2\alpha_3 + \tfrac{D}{2}(\alpha_2 + \alpha_1 - 2\alpha_3) \end{aligned} \tag{2.19}$$

$\gamma_1^{(i)}$ and $\gamma_2^{(i)}$ are the negative and nonlinear damping for oscillator i. D gives the dissipative and R the reactive coupling. When uncoupled the oscillators have a stable limit cycle with amplitude $|\alpha_1| = \bar{r_i} = \sqrt{\gamma_1^{(i)}/2\gamma_2^{(i)}}$. The system above can be written in terms of modulus and phase using $\alpha_i = r_i e^{i\phi_i}$:

$$\begin{aligned}
\dot{r}_1 &= \left(\frac{\gamma_1^{(1)}}{2} - \gamma_2^{(1)} r_1^2\right) r_1 + \frac{D}{2}(r_2\cos(\theta) + r_3\cos(\theta+\varphi) - 2r_1) \\
\dot{r}_2 &= \left(\frac{\gamma_1^{(2)}}{2} - \gamma_2^{(2)} r_2^2\right) r_2 + \frac{D}{2}(r_1\cos(\theta) + r_3\cos(\varphi) - 2r_2) \\
\dot{r}_3 &= \left(\frac{\gamma_1^{(3)}}{2} - \gamma_2^{(3)} r_3^2\right) r_3 + \frac{D}{2}(r_2\cos(\varphi) + r_1\cos(\theta+\varphi) - 2r_3) \\
\dot{\theta} &= -(\omega_2 - \omega_1) + \frac{D}{2}\left(-\left(\frac{r_1}{r_2} + \frac{r_2}{r_1}\right)\sin(\theta) + \frac{r_3}{r_2}\sin(\varphi) - \frac{r_3}{r_1}\sin(\varphi+\theta)\right) \\
\dot{\varphi} &= -(\omega_3 - \omega_2) + \frac{D}{2}\left(-\left(\frac{r_2}{r_3} + \frac{r_3}{r_2}\right)\sin(\varphi) + \frac{r_1}{r_2}\sin(\theta) - \frac{r_1}{r_3}\sin(\varphi+\theta)\right)
\end{aligned} \tag{2.20}$$

Where $\theta = \phi_2 - \phi_1$ and $\varphi = \phi_3 - \phi_2$. Assuming small coupling the dynamics of $\dot{r}_1$, $\dot{r}_2$ and $\dot{r}_3$ can be neglected [8]. Thus taking the limit cycle amplitudes we have:

$$\begin{aligned}
\dot{\theta} &= -\Delta_{2,1} + \frac{D}{2}(-2\sin(\theta) + \sin(\varphi) - \sin(\varphi+\theta)) \\
\dot{\varphi} &= -\Delta_{3,2} + \frac{D}{2}(-2\sin(\varphi) + \sin(\theta) - \sin(\varphi+\theta))
\end{aligned} \tag{2.21}$$

In this $\Delta_{i,j} = \omega_i - \omega_j$. To find phase locking in the first two oscillators of the system $\dot{\theta} = 0$ has to be possible, which requires:

$$\frac{2\Delta_{2,1}}{D} = -2\sin(\theta) + \sin(\varphi) - \sin(\varphi+\theta) \tag{2.22}$$

Where θ is a constant implying that φ can only take a few specific values, if any value at all makes the equality valid. Therefore the area in which phase locking for the first and second oscillator can occur is:

$$|\Delta_{2,1}| \leq \frac{D}{2} \max_{\theta,\varphi\in(-\pi,\pi]} \{-2\sin(\theta) + \sin(\varphi) - \sin(\varphi+\theta)\} \approx 1.760D \tag{2.23}$$

Where continuity ensures the maximum is taken and all values between this and the minimum, which is the maximum multiplied by -1, are reached since the total expression is odd in both variables. Independently the same area is found for the second phase difference φ since only the roles of θ and φ are swapped in the right-hand side of 2.23, but the domain over which the maximum was taken for both variables was equal.
Picking a value for the left hand side of 2.22 however gives a set of certain combinations of θ and φ that satisfy the equation and $\frac{2\Delta_{3,2}}{D}$ in the equation's equivalent for φ thus becomes limited to values obtained within that set. In turn this limitation might heavily restrict the values $\Delta_{3,2}$ can take, depending on the values of D and $\Delta_{2,1}$ chosen (remember constant θ requires constant φ). A nice Arnold tongue for θ in which all parameters allow the same tongue for φ is found by replacing the maximum in 2.23 by:

$$\max_{\theta,\varphi\in(-\pi,\pi]} \{\min\{-2\sin(\theta) + \sin(\varphi) - \sin(\varphi+\theta), -2\sin(\varphi) + \sin(\theta) - \sin(\varphi+\theta)\}\} \tag{2.24}$$

This ensures simultaneous phase locking can be achieved for as large of an interval for $\Delta_{i,j}$ as possible. Smaller values up until the minimum of the maximum are now also available for $\Delta_{3,2}$ for each chosen $\Delta_{2,1}$. The solution to 2.24 is found at a point where the two expressions have the same value since their range is the same on the used domain. From this it follows that the maximum is obtained with $\theta = \varphi$ or $\theta = \pi - \varphi$. The former does give the maximum. Differentiation with this in mind of one of the expressions followed by setting the result equal to zero:

$$-\cos(\theta) - 2\cos(2\theta) = 0 \tag{2.25}$$

Which gives a maximum for:

$$\theta = \varphi = -2\arctan\left(\sqrt{6 - \sqrt{33}}\right) \tag{2.26}$$

Leading to the mutual Arnold tongues given by:

$$|\Delta_{i,j}| \leq 0.880D \tag{2.27}$$

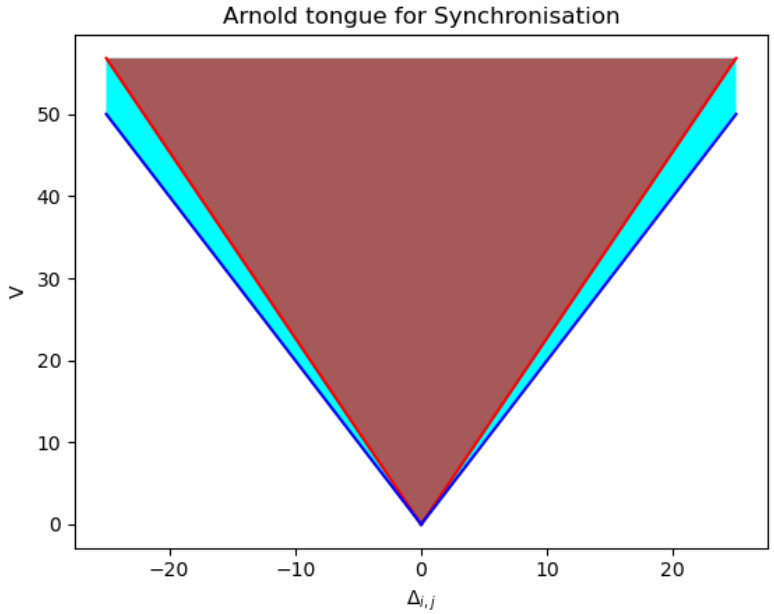

Fig. 2.6: Area for which both synchronisations can occur for the same domain of values $\Delta_{i,j}$(red) and Arnold tongue for two CVdPOs (blue). $V = 2D$

When compared to the region for which synchronisation of two oscillators occurs (fig. 2.5), the region for three oscillators appears slightly narrower.

2.3.2 Synchronisation of three chain coupled CVdPOs

Instead of 2.19, for the oscillators coupled like links in a chain, the following is used:

$$\begin{aligned}
\dot{\alpha}_1 &= -i\omega_1\alpha_1 + \tfrac{\gamma_1^{(1)}}{2}\alpha_1 - \gamma_2^{(1)}|\alpha_1|^2\alpha_1 + \tfrac{D}{2}(\alpha_2 - \alpha_1) \\
\dot{\alpha}_2 &= -i\omega_2\alpha_2 + \tfrac{\gamma_1^{(2)}}{2}\alpha_2 - \gamma_2^{(2)}|\alpha_2|^2\alpha_2 + \tfrac{D}{2}(\alpha_3 + \alpha_1 - 2\alpha_2) \\
\dot{\alpha}_3 &= -i\omega_3\alpha_3 + \tfrac{\gamma_1^{(3)}}{2}\alpha_3 - \gamma_2^{(3)}|\alpha_3|^2\alpha_3 + \tfrac{D}{2}(\alpha_2 - \alpha_3)
\end{aligned} \tag{2.28}$$

Where the second oscillator is the middle link and the first and third are its neighbours at the end of the chain. The relevant equations from the system analogous to 2.20

$$\begin{aligned}
\dot{\theta} &= -(\omega_2 - \omega_1) + \tfrac{D}{2}\left(-\left(\tfrac{r_1}{r_2} + \tfrac{r_2}{r_1}\right)\sin(\theta) + \tfrac{r_3}{r_2}\sin(\varphi)\right) \\
\dot{\varphi} &= -(\omega_3 - \omega_2) + \tfrac{D}{2}\left(-\left(\tfrac{r_2}{r_3} + \tfrac{r_3}{r_2}\right)\sin(\varphi) + \tfrac{r_1}{r_2}\sin(\theta)\right)
\end{aligned} \tag{2.29}$$

Substituting limit cycle amplitudes gives:

$$\begin{aligned}
\dot{\theta} &= -\Delta_{2,1} + \tfrac{D}{2}\left(-2\sin(\theta) + \sin(\varphi)\right) \\
\dot{\varphi} &= -\Delta_{3,2} + \tfrac{D}{2}\left(-2\sin(\varphi) + \sin(\theta)\right)
\end{aligned} \tag{2.30}$$

Once again phase locking of θ also locks φ, thus the Arnold tongue for one pair of oscillators is:

$$|\Delta_{2,1}| \leq \frac{D}{2}\max_{\theta,\varphi\in(-\pi,\pi]}\{-2\sin(\theta) + \sin(\varphi)\} = \frac{3}{2}D \tag{2.31}$$

Yet the Arnold tongue of the other pairs of oscillators do depend on the specific point in this region. Similar to in the all-to-all case it is therefore helpful to look at the biggest Arnold tongues that can be acquired simultaneously. For this region the maximum above is replaced by:

$$\max_{\theta,\varphi\in(-\pi,\pi]}\{\min\{-2\sin(\theta) + \sin(\varphi), -2\sin(\varphi) + \sin(\theta)\}\} \tag{2.32}$$

For which the maximum is found in the same way as for the all-to-all system. Hence the mutual Arnold tongues are found as:

$$|\Delta_{i,j}| \leq \frac{D}{2} \tag{2.33}$$

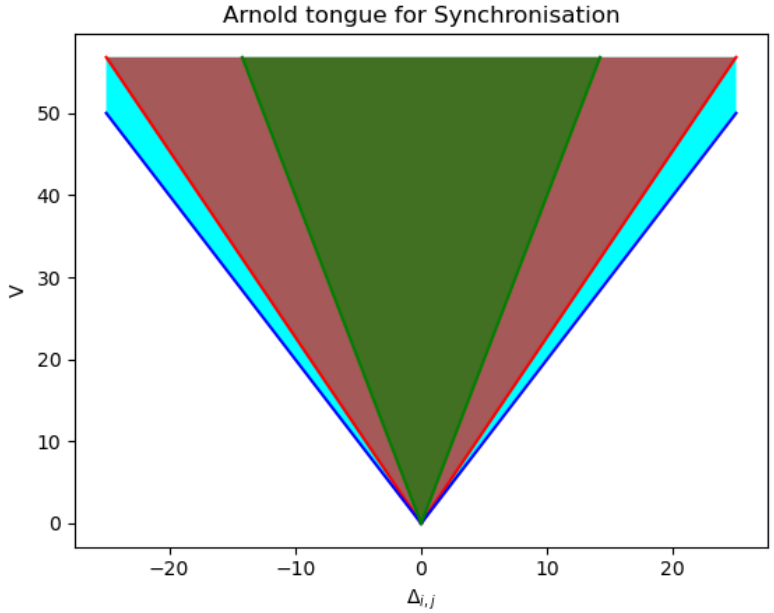

Fig. 2.7: Area for which both synchronisations can occur for the same domain of values $\Delta_{i,j}$ with chain coupling (green), all-to-all coupling (red) and for two CVdPOs (blue). $V = 2D$.

Relative to the Arnold tongue for both the 2 oscillator system and the all-to-all coupled 3 oscillator system, the area for synchronisation of a chain of 3 CVdPOs is about half as wide. Synchronisation of oscillators with indirect coupling therefore seems to be more difficult to achieve than with direct coupling.

2.4 One quantum VdP oscillator

A quantum Van der Pol oscillator can simulated using a Lindblad master equation for which [6] proposed a derivation using a heat bath. Setting $\hbar = 1$ the LME is:

$$\dot{\rho} = \mathcal{L}(\rho) = -i[H, \rho] + \gamma_{\downarrow}\mathcal{D}[a^2]\rho + \gamma_{\uparrow}\mathcal{D}[a^{\dagger}]\rho \tag{2.34}$$

Where H is the Hamiltonian of the harmonic oscillator, $H = \omega a^{\dagger}a$ with ω the eigenfrequency of the system; a the annihilation operator; $\mathcal{D}[L]\rho = L\rho L^{\dagger} - 1/2\{L^{\dagger}L, \rho\}$; ρ gives the density matrix of the VdP oscillator; $\gamma_{\downarrow}$ and $\gamma_{\uparrow}$ give the damping and pumping rate respectively.

2.4.1 Relation of the QVdP to the CVdP

The QVdPO is not directly derived from the CVdPO, however the connection between the quantum oscillator and the classical one can be shown using the complex amplitude form of the CVdPO [7]:

$$\dot{\alpha} = -i\omega\alpha + \alpha(\kappa_1 - 2\kappa_2|\alpha|^2) \tag{2.35}$$

A different way to write 2.34 dropping the shorthand notation for the dissipators is:

$$\dot{\rho} = -i[H, \rho] + \kappa_1(2a^{\dagger}\rho a - aa^{\dagger}\rho - \rho aa^{\dagger}) + \kappa_2(2a^2\rho a^{\dagger 2} - a^{\dagger 2}a^2\rho - \rho a^{\dagger 2}a^2) \tag{2.36}$$

Where $\kappa_1 = \frac{\mu}{2}$ and $\kappa_2 = \frac{\mu}{16}$ with respect to 2.1 [5], thus $\gamma_\downarrow = \frac{\mu}{8}$ and $\gamma_\uparrow = \mu$ in 2.34. Using the expression above the derivative of the expectation value for a can be found:

$$\frac{\mathrm{d}\langle a\rangle}{\mathrm{d}t} = \frac{\mathrm{d}\,\mathrm{Tr}(\rho a)}{\mathrm{d}t} = \frac{\mathrm{d}\sum_i^n \sum_j^n \rho_{i,j} a_{j,i}}{\mathrm{d}t} = \sum_i^n \sum_j^n (\frac{\mathrm{d}\rho_{i,j}}{\mathrm{d}t} a_{j,i} + \rho_{i,j} \frac{\mathrm{d}a_{j,i}}{\mathrm{d}t}) \tag{2.37}$$

Since the annihilation operator a itself is constant in time, the right most term in 2.37 equals zero and we get:

$$\frac{\mathrm{d}\langle a\rangle}{\mathrm{d}t} = \sum_i^n \sum_j^n \dot{\rho}_{i,j} a_{j,i} = \mathrm{Tr}(\dot{\rho} a) \tag{2.38}$$

Combining this with 2.36 gives:

$$\frac{\mathrm{d}\langle a\rangle}{\mathrm{d}t} = \mathrm{Tr}\{-i[H,\rho]a + \kappa_1(2a^\dagger \rho a - a a^\dagger \rho - \rho a a^\dagger)a + \kappa_2(2a^2 \rho a^{\dagger 2} - a^{\dagger 2} a^2 \rho - \rho a^{\dagger 2} a^2)a\} \tag{2.39}$$

The trace of a matrix is linear so we can rewrite this term by term, for the first expression we get:

$$\mathrm{Tr}(-i[H,\rho]a) = -i\omega(\mathrm{Tr}\big(a^\dagger a \rho a\big) - \mathrm{Tr}\big(\rho a^\dagger a^2\big)) \tag{2.40}$$

Next we use the cyclic invariance of traces and that $[a, a^\dagger] = 1$

$$\mathrm{Tr}(-i[H,\rho]a) = -i\omega(\mathrm{Tr}\big(a a^\dagger a \rho\big) - \mathrm{Tr}\big(a^\dagger a^2 \rho\big)) = -i\omega\,\mathrm{Tr}\big([a, a^\dagger] a\rho\big) = -i\omega\,\mathrm{Tr}(\rho a) = -i\omega\langle a\rangle \tag{2.41}$$

Doing the same for the second term one finds:

$$\mathrm{Tr}\big(\kappa_1(2a^\dagger \rho a - a a^\dagger \rho - \rho a a^\dagger)a\big) = \kappa_1\,\mathrm{Tr}\big(2\rho a^2 a^\dagger - \rho a^2 a^\dagger - \rho a a^\dagger a\big) = \kappa_1\,\mathrm{Tr}\big(\rho a[a, a^\dagger]\big) = \kappa_1\langle a\rangle \tag{2.42}$$

And finally for the last term:

$$\begin{aligned}
\mathrm{Tr}\big(\kappa_2(2a^2 \rho a^{\dagger 2} - a^{\dagger 2} a^2 \rho - \rho a^{\dagger 2} a^2)a\big) &= \kappa_2\,\mathrm{Tr}\big(2a\rho a^{\dagger 2} a^2 - a\rho a a^{\dagger 2} a - a\rho a^{\dagger 2} a^2 + \rho a^\dagger a a^\dagger a^2 - \rho a^\dagger a a^\dagger a^2\big) \\
&= \kappa_2\,\mathrm{Tr}\big((a^2 \rho a^\dagger + a^\dagger a^2 \rho)[a^\dagger, a]\big) \\
&= \kappa_2\,\mathrm{Tr}\big(-2a^\dagger a^2 \rho\big) \\
&= -2\kappa_2\langle a^\dagger a^2\rangle
\end{aligned} \tag{2.43}$$

From combining all these terms it follows that:

$$\frac{\mathrm{d}\langle a\rangle}{\mathrm{d}t} = -i\omega\langle a\rangle + \kappa_1\langle a\rangle - 2\kappa_2\langle a^\dagger a^2\rangle \tag{2.44}$$

Replacing operator a with the complex number α for a coherent state in the classical limit ($\gamma_\downarrow \to 0$) gives the complex amplitude equation for the classical VdP oscillator 2.35 [7].

2.4.2 Long term behaviour of the QVdP

For the inquiry into the long term behaviour of the QVdPO the functions 'steadystate' and 'mesolve' from the QuTiP package were used[13]. In [6] the steady-state in the quantum limit, $\gamma_\downarrow \to \infty$, of 2.36 is found to be $\rho_s = \frac{2}{3}|0\rangle\langle 0| + \frac{1}{3}|1\rangle\langle 1|$ as can be verified by plugging this matrix into the spin representation of 2.36 as obtained in appendix A:

$$\dot{\rho} = -i[H,\rho] + \kappa_1(2\sigma^+ \rho \sigma^- - \sigma^- \sigma^+ \rho - \rho \sigma^- \sigma^+) + 2\kappa_1(2\sigma^- \rho \sigma^+ - \sigma^+ \sigma^- \rho - \rho \sigma^+ \sigma^-) \tag{2.45}$$

Where the Hamiltonian is $H = \omega\sigma^+\sigma^-$, and the spin flip operators are defined as $\sigma^+ = |1\rangle\langle 0|$ and $\sigma^- = |0\rangle\langle 1|$. For the steady-state the right-hand side then needs to become zero, as it does for ρ_s:

$$\dot{\rho_s} = -i\omega\left(\frac{1}{3}\left|1\right\rangle\left\langle 1\right| - \frac{1}{3}\left|1\right\rangle\left\langle 1\right|\right) + \kappa_1\left(\frac{4}{3}\left|1\right\rangle\left\langle 1\right| - \frac{2}{3}\left|0\right\rangle\left\langle 0\right| - \frac{2}{3}\left|0\right\rangle\left\langle 0\right|\right) + 2\kappa_1\left(\frac{2}{3}\left|0\right\rangle\left\langle 0\right| - \frac{1}{3}\left|1\right\rangle\left\langle 1\right| - \frac{1}{3}\left|1\right\rangle\left\langle 1\right|\right) = 0 \tag{2.46}$$

Which is obtained using that the product of a bra and a ket equal the Kronecker delta taking value 1 for equal Fock states and zero otherwise: $\langle n|m\rangle = \delta_{n,m}$.
Through QuTiP the same steady-state is observed:

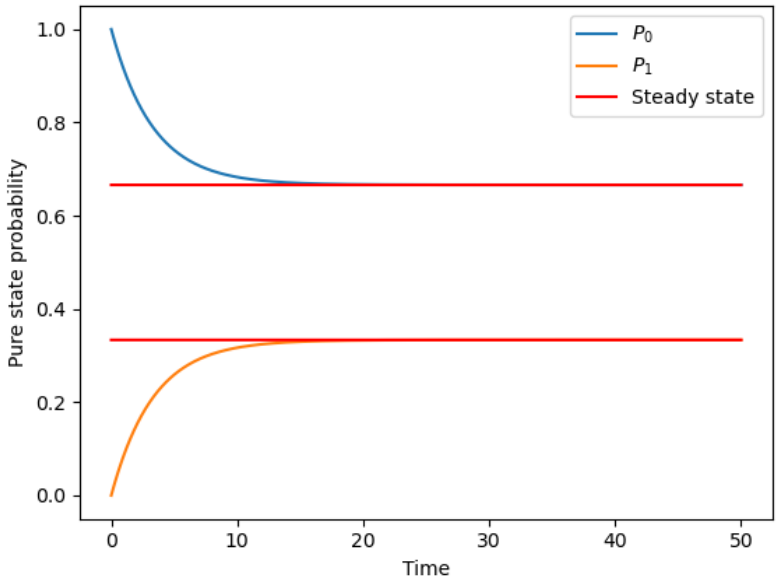

Fig. 2.8: Plot showing the steady-state solution for a Quantum Van der Pol oscillator and the shift of the solution of the master equation towards that, $\omega = 1, \gamma_\downarrow = 100, \gamma_\uparrow = 0.1$.

In fig. 2.8 the convergence of the probabilities to find the oscillator in Fock state 0 or 1 can be seen to converge quite rapidly to the steady-state. Whilst the system theoretically has infinitely many Fock states, in the quantum limit only the lowest two states are occupied as explained in appendix A. To check the validity of the two-state approximation higher states can be taken into account and the discrepancy between finding the system in one of the lowest two states and the total probability of 1 can be found. In the case of fig. 2.8 with 10 states per oscillator, both the 'steadystate' and the 'mesolve' function give a difference of 0.00033, which is negligible. When $\gamma_\uparrow \geq \gamma_\downarrow$ higher states of the system also become occupied and the two-state approximation brakes down. Even though the probabilities remain fixed in the steady-state, the system does still exhibit stable oscillation akin to the limit cycle found in the CVdP. The oscillations can be seen for instance using the Wigner function, which gives a quasi-probability distribution for the location and momentum of the oscillator. The Wigner function is defined as:

$$W(x,p) = \frac{1}{\hbar\pi}\int_{-\infty}^{\infty}\left\langle x+y\right|\hat{\rho}\left|x-y\right\rangle e^{-2ipy/\hbar}dy \tag{2.47}$$

For x relative to $x_{zpf} = \frac{1}{\sqrt{2m\omega}}$ and p to $p_{zpf} = \sqrt{m\omega/2}$, values for the zero-point fluctuations [9]. The distribution, when viewed analogously to a phase diagram, clearly indicates oscillations. Its shape is a circle with symmetrical values, for which the top half has positive momentum, thus increasing x/x_{zpf} and the bottom half has negative momentum, decreasing x/x_{zpf}:

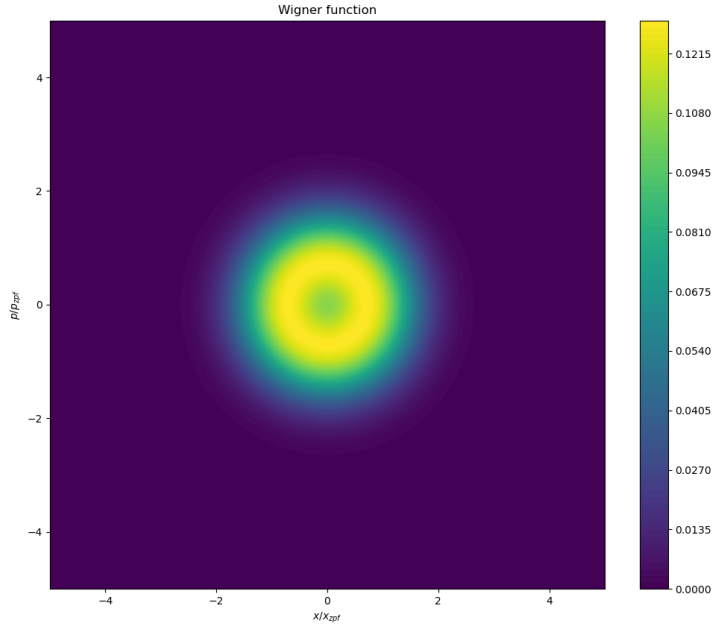

Fig. 2.9: Colourmap of the Wigner function for the one QVdP oscillator steady-state in the quantum limit with 5 simulated states, $\omega = 1$, $\gamma_\downarrow = 100$, $\gamma_\uparrow = 0.1$.

2.5 Two coupled QVdP oscillators

The Lindblad master equation for two coupled quantum Van der Pol oscillators is:

$$\dot{\rho} = \mathcal{L}(\rho) = -i[H, \rho] + V\mathcal{D}[a_1 - e^{i\theta}a_2]\rho + \sum_{i=1}^{2} \gamma_\downarrow^{(i)}\mathcal{D}[a_i^2]\rho + \gamma_\uparrow^{(i)}\mathcal{D}[a_i^\dagger]\rho \tag{2.48}$$

Where $H = \sum_{i=1}^{2} \omega_i a_i^\dagger a_i$, the subscripts and superscripts indicate for which of the two oscillators an operator or constant holds and V gives the coupling strength of the oscillators. θ in the dissipator of the coupling determines the phase difference for which the largest coupling takes place and in that way gives the phase difference with which synchronisation may occur. In the quantum limit, $\gamma_\downarrow \to \infty$, the two- and three-oscillator systems occupy a limited number of their infinite Fock states, as explained below. For those systems, we thus look at their dynamics in the quantum limit to keep the analysis manageable.

2.5.1 Steady-state of two coupled QVdPOs

As a starting point for analysis of the coupled system, the steady-state of 2.48 can be used. To obtain this solution we look at oscillators in the quantum limit, $\gamma_\downarrow \to \infty$, with equal damping and pumping rates for the oscillators: $\gamma_{\uparrow,\downarrow}^{(1)} = \gamma_{\uparrow,\downarrow}^{(2)}$. In this case only the first and second Fock states of the oscillators are occupied because higher states are annihilated by non-linear damping. The two-state system can be mapped to a spin system with an up $|\uparrow\rangle$ and down $|\downarrow\rangle$ state corresponding to $|1\rangle$ and $|0\rangle$ respectively[7](for the connection between the representations see Appendix A):

$$\dot{\rho} = \mathcal{L}(\rho) = -i[H, \rho] + V\mathcal{D}[\sigma_1^- - e^{i\theta}\sigma_2^-]\rho + \sum_{i=1}^{2} 2\gamma_\uparrow^{(i)}\mathcal{D}[\sigma_i^-]\rho + \gamma_\uparrow^{(i)}\mathcal{D}[\sigma_i^+]\rho \tag{2.49}$$

Here $H = \sum_{i=1,2} \omega_i \sigma_i^+ \sigma_i^-$, the original ladder operators a_i and $a_i^\dagger$ are replaced by spin operators $\sigma_i^- = |0\rangle\langle 1|_i$ and $\sigma_i^+ = |1\rangle\langle 0|_i$. The spin operators for the combined system are $\sigma_1^\pm = \sigma_1^\pm \otimes I_2$ and

$\sigma_2^{\pm} = I_2 \otimes \sigma_2^{\pm}$, with the Kronecker product $\otimes$. The density matrix of the system is written in a similar way: $\rho = \rho_1 \otimes \rho_2 = |\cdot\rangle\langle\cdot|_1 \otimes |\cdot\rangle\langle\cdot|_2$, where either the up or down state can be inserted for each dot separately. The steady-state solution of 2.49 is the density matrix obtained using these operators when solving $\mathcal{L}(\pi) = 0$. The resulting matrix is:

$$\begin{aligned} \pi_{1,1} &= 1 - \tfrac{\gamma_\uparrow(5\gamma_\uparrow+2V)(\Delta\omega^2+(3\gamma_\uparrow+V)^2)}{N} \\ \pi_{2,2} = \pi_{3,3} &= \tfrac{\gamma_\uparrow(2\gamma_\uparrow+V)(\Delta\omega^2+(3\gamma_\uparrow+V)^2)}{N} \\ \pi_{4,4} &= \tfrac{\gamma_\uparrow^2(\Delta\omega^2+(3\gamma_\uparrow+V)^2)}{N} \\ \pi_{2,3} = \pi_{3,2}^* &= \tfrac{\gamma_\uparrow V(\gamma_\uparrow+V)(3\gamma_\uparrow+V-i\Delta\omega)e^{-i\theta}}{N} \end{aligned} \tag{2.50}$$

Where $N = (\gamma_\uparrow + V)(3\gamma_\uparrow(\Delta\omega^2 + 9\gamma_\uparrow) + (\Delta\omega^2 + 27\gamma_\uparrow^2)V + 8\gamma_\uparrow V^2)$ and the unmentioned elements are equal to zero.
As initial wave vectors for the Monte Carlo simulation proposed later on, samples from the steady-state are used: $\pi = \sum_n P(\pi_n)|\pi_n\rangle\langle\pi_n|$. For the π_n wave functions normed eigenvectors of the π density matrix (pure states) are used and $P(\pi_n)$ is equal to the respective eigenvalue, all of which sum to one since the sum equals the trace of the density matrix.

$$\pi_1 = \begin{pmatrix}1\\0\\0\\0\end{pmatrix}, \pi_2 = \tfrac{1}{\sqrt{2}}\begin{pmatrix}0\\-\frac{\pi_{2,3}}{|\pi_{2,3}|}\\1\\0\end{pmatrix}, \pi_3 = \tfrac{1}{\sqrt{2}}\begin{pmatrix}0\\\frac{\pi_{2,3}}{|\pi_{2,3}|}\\1\\0\end{pmatrix}, \pi_4 = \begin{pmatrix}0\\0\\0\\1\end{pmatrix} \tag{2.51}$$

$$P(\pi_1) = \pi_{1,1}, P(\pi_2) = -|\pi_{2,3}| + \pi_{2,2}, P(\pi_3) = |\pi_{2,3}| + \pi_{2,2}, P(\pi_4) = \pi_{4,4}$$

2.5.2 Trajectories of two coupled QVdPOs

For the investigation into synchronisation of the two coupled quantum VdP oscillators we look at quantum trajectories. These offer more insight into single realisations of quantum processes as opposed to considering averages only. The Lindblad master equation for the coupled oscillators 2.36 can be used to obtain the stochastic Schrödinger equation for the coupled system [2]:

$$d|\psi(t)\rangle = dt\left[-iH_{eff} + \sum_k \frac{\langle X_k\rangle_{\psi(t)}}{2}\left(L_k - \frac{\langle X_k\rangle_{\psi(t)}}{4}\right)\right]|\psi(t)\rangle + \sum_k \mathrm{d}W_k(t)\left(L_k - \frac{\langle X_k\rangle_{\psi(t)}}{2}\right)|\psi(t)\rangle \tag{2.52}$$

Here $H_{eff} = H - i\sum_k L_k^\dagger L_k/2$, $X_k = L_k + L_k^\dagger$, with H the original Hamiltonian of the system, $\langle A\rangle_{\psi(t)} \equiv \langle\psi(t)|A|\psi(t)\rangle$. The sums are taken over the Lindblad operators: $L_1 = \sqrt{\gamma_\downarrow^{(1)}}a_1^2$, $L_2 = \sqrt{\gamma_\uparrow^{(1)}}a_1^\dagger$, $L_3 = \sqrt{\gamma_\downarrow^{(2)}}a_2^2$, $L_4 = \sqrt{\gamma_\uparrow^{(2)}}a_2^\dagger$ and the operator describing the coupling $L_5 = \sqrt{V}(a_1 - e^{i\theta}a_2)$, obtained from 2.36. $\mathrm{d}W_k$ is a Wiener stochastic increment, which is introduced by the continuous measurement of X_k. The increments have Gaussian behaviour and zero mean over trajectories, $\langle \mathrm{d}W_k\rangle = 0$, with $\mathrm{d}W_k^2 = \mathrm{d}t$.

2.6 Three coupled QVdP oscillators

Here the two systems possible with three coupled QVdPOs are presented. These are the all-to-all coupled system, in which all oscillators are directly linked and the chain coupled system, in which one oscillator is the forms the link between the other two.

2.6.1 Three all-to-all coupled QVdPOs

The system of three all-to-all coupled QVdP oscillators is given by:

$$\dot\rho = \mathcal{L}(\rho) = -i[H,\rho] + V(\mathcal{D}[a_1 - e^{i\theta}a_2] + \mathcal{D}[a_2 - e^{i\theta}a_3] + \mathcal{D}[a_1 - e^{i\theta}a_3])\rho + \sum_{i=1}^{3}\gamma_\downarrow^{(i)}\mathcal{D}[a_i^2]\rho + \gamma_\uparrow^{(i)}\mathcal{D}[a_i^\dagger]\rho \tag{2.53}$$

Where $H = \sum_{i=1}^{3} \omega_i a_i^\dagger a_i$, the subscripts and superscripts indicate for which of the three oscillators an operator or constant holds and V gives the coupling strength of the oscillators. In a similar way to what was done before, this system as well can be cast into a spin equation since only two states are occupied per oscillator in the quantum limit. However finding the steady-state matrix now proves quite tricky, luckily this can be found relatively easily numerically once the system parameters are known. The eigendecomposition of the steady-state is then again used as a distribution for the initial states of the Monte Carlo simulation. 2.53 Is also the starting point to find a stochastic Schrödinger equation of the shape of 2.52. For this SSE Lindbladians $L_6 = \sqrt{\gamma_\downarrow^{(3)}} a_3^2$, $L_7 = \sqrt{\gamma_\uparrow^{(3)}} a_3^2\dagger$, $L_8 = \sqrt{V}(a_1 - e^{i\theta} a_3)$ and $L_9 = \sqrt{V}(a_2 - e^{i\theta} a_3)$ are added and the original Hamiltonian gets an extra term $\omega_3 a_3^\dagger a_3$.

2.6.2 Three chain coupled QVdPOs

The chain coupled system of three QVdPOs is very similar to the all-to-all coupled system presented above. It misses the link between oscillator 1 and 3 giving it the structure of a chain:

$$\dot{\rho} = \mathcal{L}(\rho) = -i[H, \rho] + V(\mathcal{D}[a_1 - e^{i\theta} a_2] + \mathcal{D}[a_2 - e^{i\theta} a_3])\rho + \sum_{i=1}^{3} \gamma_\downarrow^{(i)} \mathcal{D}[a_i^2]\rho + \gamma_\uparrow^{(i)} \mathcal{D}[a_i^\dagger]\rho \tag{2.54}$$

2.7 Quantum indicators

To investigate the synchronisation of coupled quantum VdP oscillators there are a couple of different indicators, all of which have their own characteristics. The first indicator is the complex correlator defined as[2]:

$$C_{\psi i,j}(t) = \frac{\left\langle a_i^\dagger a_j \right\rangle_{\psi(t)}}{\sqrt{\left\langle a_i^\dagger a_i \right\rangle_{\psi(t)} \left\langle a_j^\dagger a_j \right\rangle_{\psi(t)}}} \tag{2.55}$$

The modulus of this correlator gives a sense of how strong synchronisation is between the oscillators, 1 giving total correlation and 0 indicating completely uncorrelated oscillations. The phase of the correlator holds information about the phase difference of the oscillators when these are correlated. When looking at the two oscillator system for example, substituting the spin operators into 2.55 and using the values for π the following is obtained:

$$C_\pi = \frac{\pi_{2,3}}{\sqrt{(\pi_{3,3} + \pi_{4,4})(\pi_{2,2} + \pi_{4,4})}} = \frac{V(\gamma_\uparrow + V)}{(3\gamma_\uparrow + V)\sqrt{\Delta\omega^2 + (3\gamma_\uparrow + V)^2}} e^{i\Delta\phi_\pi} \tag{2.56}$$

$|C_\pi|$ can then be used to find the strength of synchronisation for both VdP oscillators for various values of $\Delta\omega$ and V, giving the quantum equivalent of the Arnold tongue as later on presented in the results section.
Another measure of synchronisation is the Pearson correlation coefficient:

$$r_{XY} = \frac{\mathrm{Cov}(X, Y)}{\sigma(X)\sigma(Y)} = \frac{\mathrm{E}[(X - \mathrm{E}[X])(Y - \mathrm{E}[Y])]}{\sqrt{\mathrm{E}(X - [X])^2 \mathrm{E}(Y - \mathrm{E}[Y])^2}} \tag{2.57}$$

In the case where the two variables are measurements of trajectories, the coefficient will depend on time and on the window used to determine the averages that replace the expectation values:

$$\begin{aligned} r_{x_1,x_2}(t|\Delta t) &= \frac{\overline{\delta\langle x_1\rangle \delta\langle x_2\rangle}}{\sqrt{\overline{\delta\langle x_1\rangle^2}\ \overline{\delta\langle x_2\rangle^2}}} \\ &= \frac{\int_{t-\Delta t/2}^{t+\Delta t/2} \left(\langle x_1 \rangle_{\psi(s)} - \frac{1}{\Delta t} \int_{s-\Delta t/2}^{s+\Delta t/2} \langle x_1 \rangle_{\psi(r)} dr \right) \left(\langle x_2 \rangle_{\psi(s)} - \frac{1}{\Delta t} \int_{s-\Delta t/2}^{s+\Delta t/2} \langle x_2 \rangle_{\psi(r)} dr \right) ds}{\sqrt{\int_{t-\Delta t/2}^{t+\Delta t/2} \left(\langle x_1 \rangle_{\psi(s)} - \frac{1}{\Delta t} \int_{s-\Delta t/2}^{s+\Delta t/2} \langle x_1 \rangle_{\psi(r)} dr \right)^2 ds \int_{t-\Delta t/2}^{t+\Delta t/2} \left(\langle x_2 \rangle_{\psi(s)} - \frac{1}{\Delta t} \int_{s-\Delta t/2}^{s+\Delta t/2} \langle x_2 \rangle_{\psi(r)} dr \right)^2 ds}} \end{aligned} \tag{2.58}$$

Where sample means are taken over a time interval Δt symmetrically around each chosen time. $x_i = (a_i + a_i^\dagger)/\sqrt{2}$ are the position quadratures of the oscillators, the expectation values of which can be

thought of as the position of the oscillators at a specific time.
Another interesting phenomenon that occurs in a system of coupled quantum oscillators is entanglement. Since the state of the system remains pure for the system governed by the stochastic Schrödinger equations as presented before, the Von Neumann entropy is an indicator of entanglement for the state of a single oscillator. This entropy is given by:

$$S_\psi = -\operatorname{Tr}[\rho_{\psi 1}(t)\log(\rho_{\psi 1}(t))] \tag{2.59}$$

Where $\rho_{\psi 1}(t)$ is the reduced density matrix of the first oscillator and the logarithm is taken of this matrix. $\rho_{\psi 1}(t)$ is found by tracing out the second oscillator using the partial trace:

$$\begin{aligned}\rho_{\psi 1}(t) &= \operatorname{Tr}_2[|\psi(t)\rangle\langle\psi(t)|] = \operatorname{Tr}_2[\rho_\psi(t)] \\ &= \begin{bmatrix}\langle 0,0|\rho_\psi(t)|0,0\rangle + \langle 0,1|\rho_\psi(t)|0,1\rangle & \langle 0,0|\rho_\psi(t)|1,0\rangle + \langle 0,1|\rho_\psi(t)|1,1\rangle \\ \langle 1,0|\rho_\psi(t)|0,0\rangle + \langle 1,1|\rho_\psi(t)|0,1\rangle & \langle 1,0|\rho_\psi(t)|1,0\rangle + \langle 1,1|\rho_\psi(t)|1,1\rangle\end{bmatrix}\end{aligned} \tag{2.60}$$

In this the ones and zeros give the numbers of the Fock states for the combined system. The partial trace in general works by adding the elements of the original matrix with the needed Fock state for the remaining oscillator and Fock states in the bra and ket for each oscillator that is traced out that are equal for the single oscillators. An example for a three oscillator system, in which the oscillators have two Fock states and the second and third oscillator are traced out, would be:

$$\langle 0|\rho|1\rangle = \langle 0,0,0|\rho|1,0,0\rangle + \langle 0,0,1|\rho|1,0,1\rangle + \langle 0,1,0|\rho|1,1,0\rangle + \langle 0,1,1|\rho|1,1,1\rangle \tag{2.61}$$

The maximum of the indicator in 2.59 is $\log(2)$ or approximately 0.69, achieved for a maximally entangled state. The value 0 is taken for states which are not entangled.

3 Results

In this section the results of various simulations for two- and three-QVdP oscillator systems will be presented. First the regions in which synchronisation is expected to occur are presented. Parameters specifically picked within or outside these regions are then used in the simulations of trajectories. For a single trajectory we show the behaviour of the four indicators. These indicators are then used, in a similar way as was done by [2], to explore the behaviour of the two-oscillator system with regard to synchronisation and entanglement. The distributions for the indicator values averaged over single trajectories are presented for two- and three-oscillator systems and a comparison between the behaviour shown by the systems is made. The code for the simulations can be found in [14]

3.1 Arnold tongues

To find parameter values for which the oscillators are expected to show synchronisation, 2.55 is used to find quantum Arnold tongues:

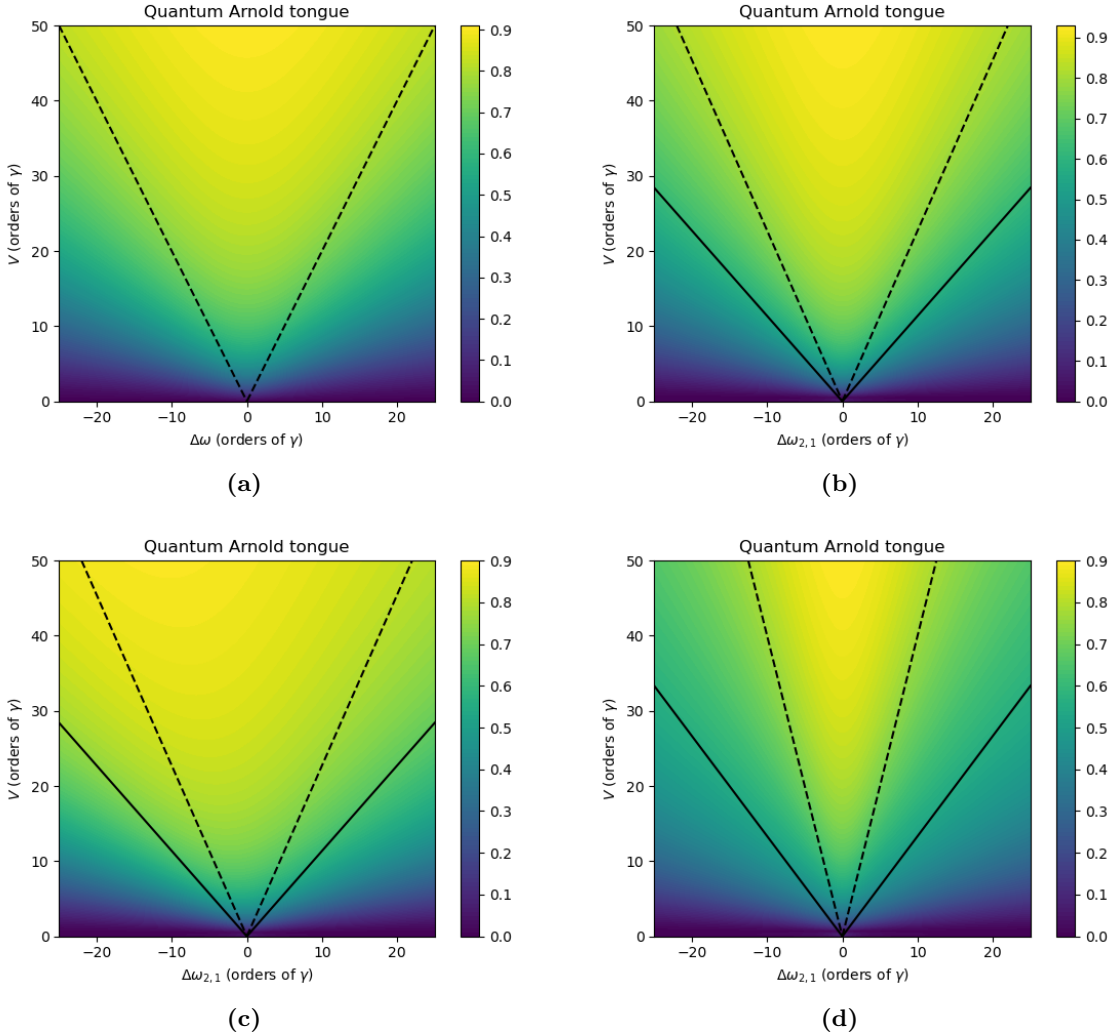

Fig. 3.1: $|C_\pi|$ for a 2- (a) and 3-oscillator system (b-d). The dotted line is the classical Arnold tongue (for three oscillators the simultaneous one) and the black line represents the largest tongue for a single pair of classical oscillators. $\gamma_\uparrow = 0.01$, (b) and (c) are all-to-all coupled, (d) is chain coupled, $\Delta\omega_{3,2} = \Delta\omega_{2,1}$ for (b) and (d), $\Delta\omega_{3,2} = \frac{V}{2.2}$ for (c).

Looking at the quantum Arnold tongues in fig. 3.1 the requirements for synchronisation in a classical system give a pretty good indication of the quantum system's behaviour. Even though the quantum

Arnold tongues are a lot smoother, their shapes and areas of strong synchronisation are very similar to their classical counterparts. The tongues of three-oscillator systems are smaller than that of the two-oscillator system, sheerly due to the need for simultaneous synchronisation of more oscillators. Here the type of coupling comes in to play as well and makes that the tongue in (d) is a lot narrower than that in (b). This difference in width is caused by the absence of one connection in the chain-coupling versus the all-to-all coupling. Without it a weaker pull towards the overall average of the system is achieved, since two links are moving the system to possibly different averages of oscillator pairs, but a third link to draw those nearer to one another is missing.
The dependence of the Arnold tongue for an oscillator pair on the $\Delta\omega$ of the other pair can be seen in (c). There eigenfrequency differences in the second pair along the edge of the classical prediction for the tongue, result in a clearly skewed synchronisation area, signalling that the conditions on both oscillator pairs are intertwined.
Utilising the knowledge obtained from these Arnold tongues, parameters within or outside of the regions can be picked when simulating the quantum systems to either enable or prevent synchronisation.

3.2 Indicator behaviour for single trajectories

Next we seek to explore the behaviour of the indicators discussed in section 2.7. To see how these indicators behave, they can be applied to a single trajectory developing from one of the eigenvectors of the steady state:

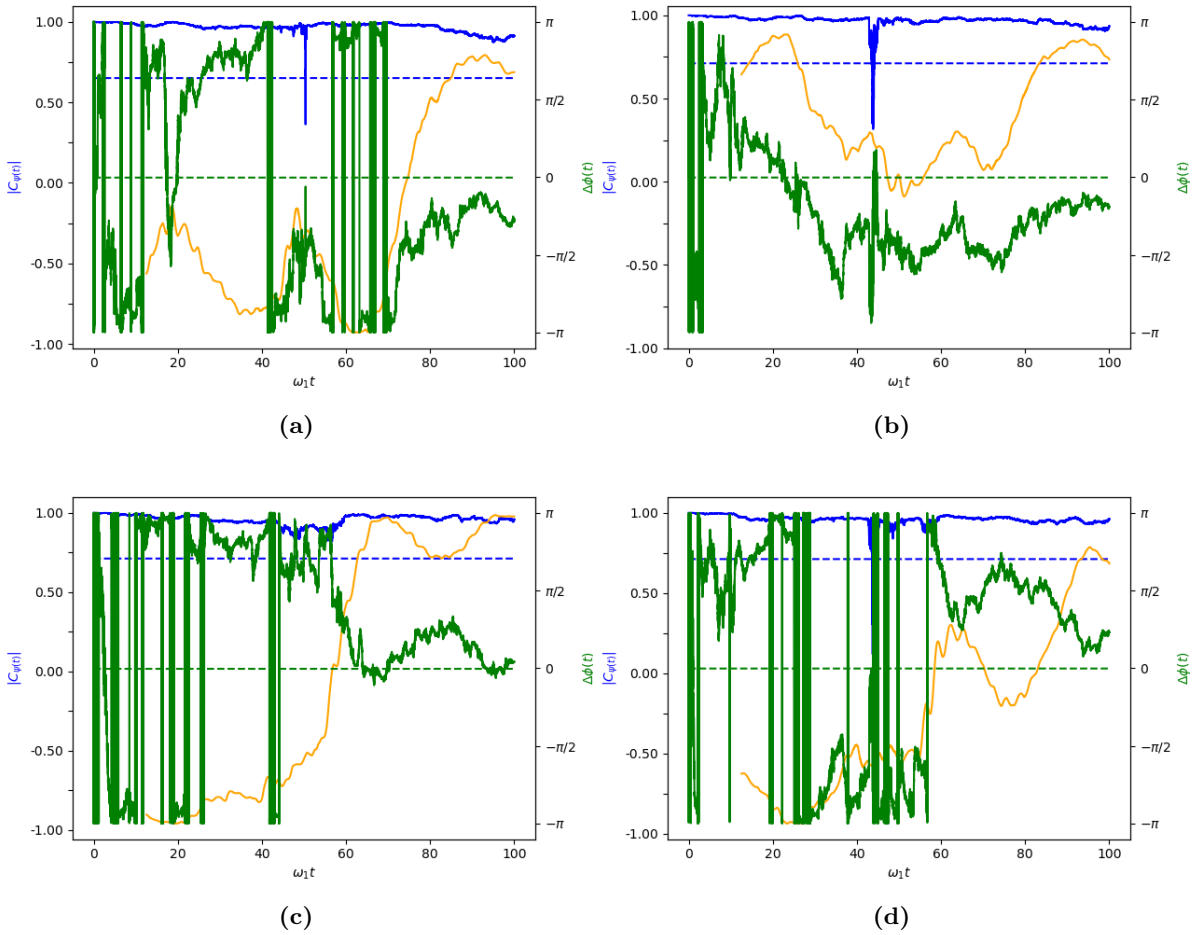

Fig. 3.2: Indicators $|C_\psi|$ (blue), $\Delta\phi_\psi$ (green) and $r_{x_i x_j}$ (orange) for a single trajectory of a two- (a) and a three-oscillator all-to-all coupled system ((b): pair 1,2; (c): pair 1,3; (d): pair 2,3). Dotted lines give the expectation values for the steady state. $\Delta\omega_{2,1} = 0.1\gamma_\uparrow (= \Delta\omega_{3,2})$, $\omega_1 = 2\pi$, $V = 10\gamma_\uparrow$, $\gamma_\uparrow = 0.01$, $\Delta t = 4\pi/\omega_1$, $\theta = 0$.

The behaviours of the indicators obtained for the two- and three-oscillator system, visible in fig. 3.2, are very similar and agree with the characteristics of the indicators found in [2]. As noted there, a high value of $|C_\psi|$ is needed for synchronisation, but other indicators should also be used, since a high value is not necessarily caused by synchronisation and thus the information contained in $\Delta\phi_\psi$ is not always high.
The angle of the coupling was set to zero, therefore phase locking was expected at $\Delta\phi_\psi = 0$. Nevertheless the coupling was picked to be weak, so as to allow the relative phases within the systems to evolve over time between the maximum and minimum phase difference. It is worth noting that the jumps in the green graphs are not actually jumps, but changes in the phase difference that increase or decrease its value above or below the maximum or minimum of the indicator respectively, lowering the absolute difference again.
Values of the phase difference around zero are accompanied by values of the Pearson correlator close to one, indicating positive linear correlation as expected. When the phase difference increases, r first drops to 0 and then goes down to -1 as the oscillators become negatively correlated. Because the Pearson correlator requires a window around the point for which it is calculated, the orange graph begins only after half of this window has passed.
Average values found in π are in line with the angle $\theta = 0$ and the indicators for the chain coupled three-oscillator system behave in the familiar way.

3.3 Monte Carlo simulations of two QVdPOs

Now we proceed with Monte Carlo simulations of 1000 trajectories per combination of parameters, initiated from the eigenvectors of the steady state randomly picked with the eigenvalues as probabilities. By averaging over these trajectories, the partially stochastic steady-state dynamics can be explored using distributions for the average indicator values. To make measurements mainly reflect the system dynamics, the oscillators are first left to depart from the eigenvectors for some time. Then the indicators are applied at each time step and averaged over the duration of the used part of a trajectory. Following this method for $\Delta\phi_\psi$ and $|C_\psi|$ the role of the coupling strength, V, becomes apparent:

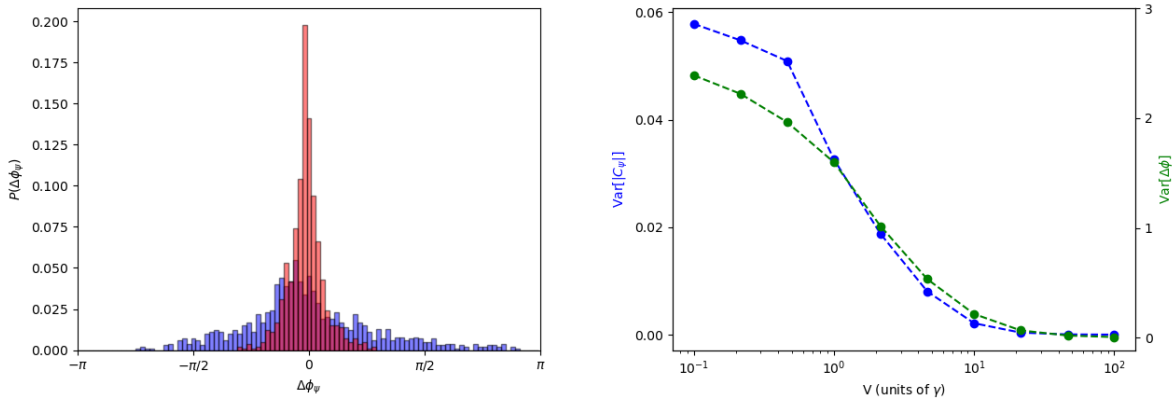

(a) **(b)**

Fig. 3.3: (a) Probability distribution of $\Delta\phi_\psi$ for the two QVdPO system with $V = \{$blue: $5\gamma_\uparrow$, red: $50\gamma_\uparrow\}$. (b) Variances for two QVdPOs of $|C_\psi|$ (blue) and $\Delta\phi_\psi$ (green). $\Delta\omega = \gamma_\uparrow$, $\omega_1 = 8\pi$, $\gamma_\uparrow = 0.01$, $\theta = 0$.

In fig. 3.3 the probability distribution of $\Delta\phi_\psi$ and the variances of $\Delta\phi_\psi$ and $|C_\psi|$ show that higher values for V lead to sharper peak in the distribution of the phase difference around value chosen through $\theta = 0$. As V increases both variances go to zero giving a strong indication of long periods of synchronisation. Even for weaker coupling the distribution in (a) shows a tendency of the system to synchronisation, be it for shorter durations.
The influence of θ on synchronisation in the system becomes clear when a few different values for it are picked when simulating the two-oscillator system:

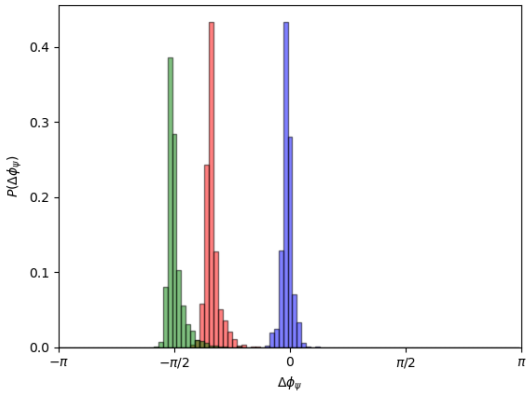

Fig. 3.4: Probability distributions for $\Delta\phi_\psi$, $V = 100\gamma_\uparrow$, $\Delta\omega = \gamma_\uparrow$, $\omega_1 = 8\pi$, $\gamma_\uparrow = 0.01$, $\theta = \{$blue: 0, red: $\pi/3$, green: $\pi/2\}$

A change in the coupling angle, θ, shifts the peak of the distribution of $\Delta\phi_\psi$ in fig. 3.4 towards the opposite of that angle. The distributions for non-zero angles are a little skewed towards zero since there are more phase differences to randomly take to the right then there are to the left.

Comparing the indicator for the entanglement of the quantum system, S_ψ, with the ones used above, correlations between synchronisation and entanglement can be explored:

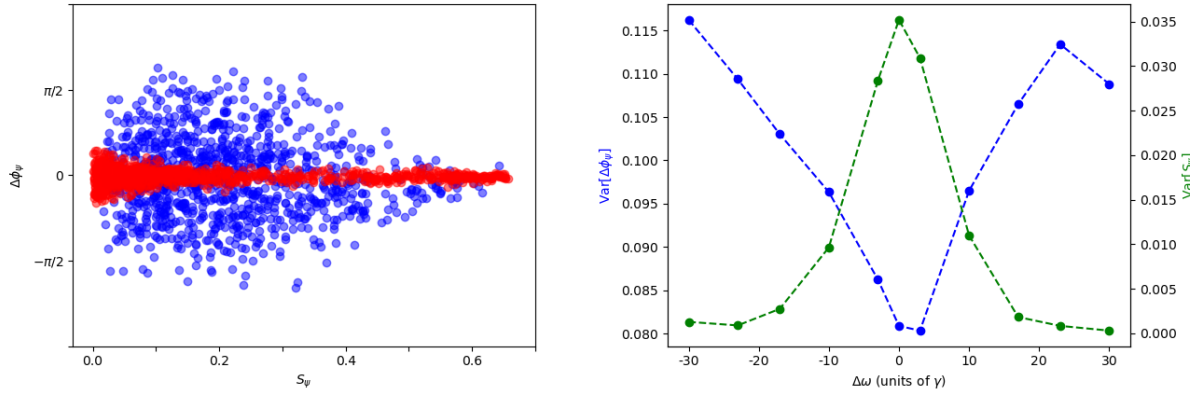

(a) **(b)**

Fig. 3.5: (a) Scatter plot of S_ψ and $\Delta\phi_\psi$ $V = \{$blue: $5\gamma_\uparrow$, red: $50\gamma_\uparrow\}$, $\Delta\omega = \gamma_\uparrow$. (b) Variances of $\Delta\phi_\psi$ (blue) and S_ψ (green), $V = 20\gamma_\uparrow$, $\Delta\omega = \{-30, -23, -17, -10, -3, 0, 3, 10, 17, 23, 30\}\gamma_\uparrow$. $\omega_1 = 8\pi$, $\gamma_\uparrow = 0.01$, $\theta = 0$.

The data displayed in fig. 3.5 shows the same correlation between synchronisation and entanglement as found in [2]. In (a) for stronger coupling more trajectories show smaller phase differences, which are accompanied by larger values for S_ψ. In general with stronger coupling high S_ψ values are also achieved more frequently. Intuitively this makes sense because stronger coupling increases the dependence of an oscillator's dynamics on the dynamics of the oscillator it is coupled to. This would not only be able to cause the dynamics to be driven towards their average, achieving synchronisation, but also introduce more co-dependence of the oscillators' states, creating more entanglement.
Furthermore, opposite behaviour of the variances of $\Delta\phi_\psi$ and S_ψ shown in (b) supports the connection between synchronisation and entanglement as well. There changes in the difference of the oscillators' natural frequencies cause the variance of $\Delta\phi_\psi$ to drop and S_ψ to rise as $\Delta\omega$ becomes close to zero. Good conditions for synchronisation thus seem to enable entanglement alongside synchronisation.

3.4 Comparing the 2- and 3-oscillator system

With the four indicators applied above, a comparison between the 2-, all-to-all coupled 3- and chain coupled 3-oscillator system will now be made. Histograms for oscillator pair 2-3 are left out as symmetry within the systems causes these to be almost completely identical to those of pair 1-2.

3.4.1 $|C_\psi|$ distributions

Starting with the distributions for $|C_\psi|$:

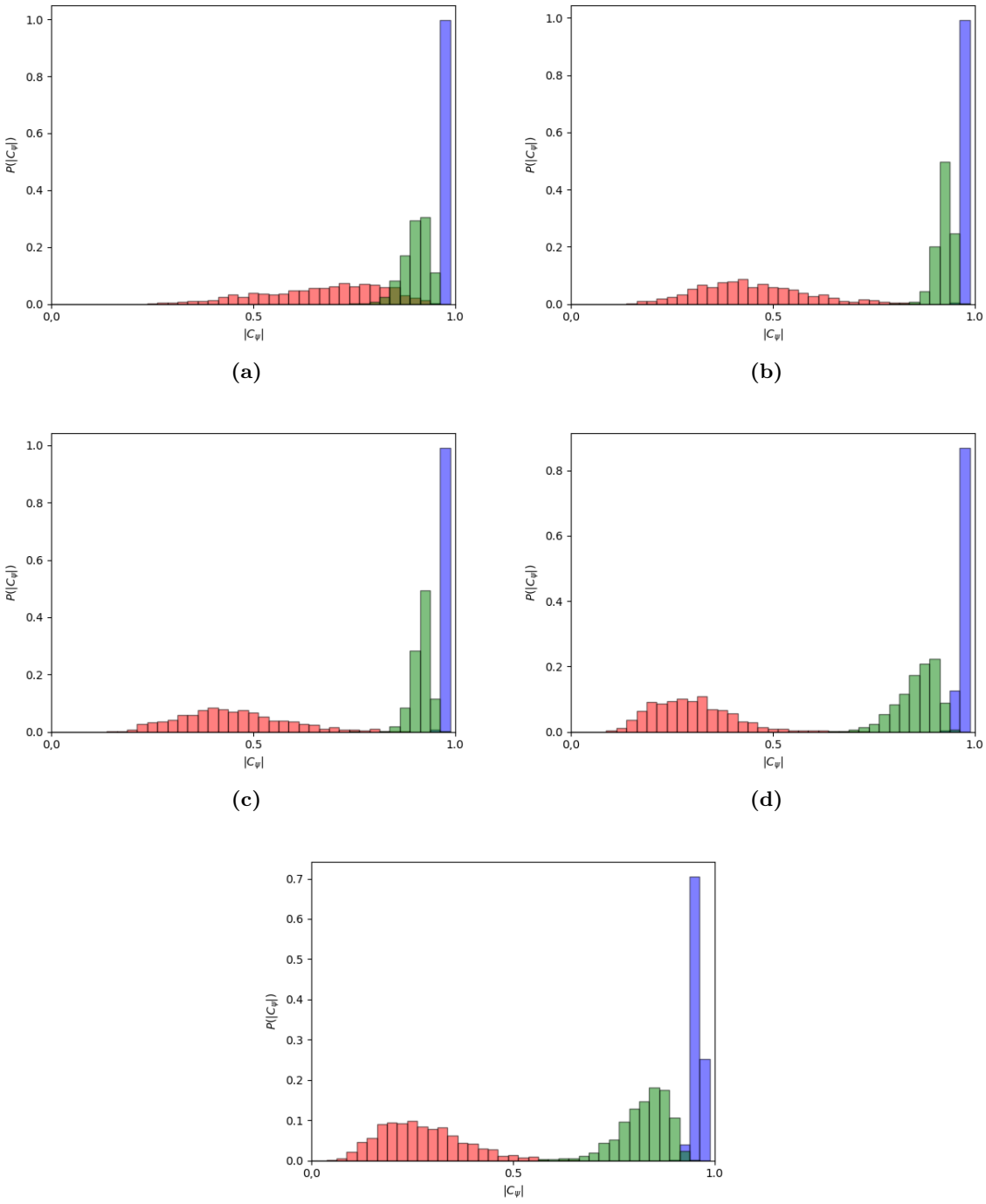

Fig. 3.6: Probability distribution of $|C_\psi|$ for different oscillator pairs. 2QVdPOs: (a); 3 all-to-all coupled QVdPOs: (b) 1-2, (c) 1-3; 3 chain coupled QVdPOs: (d) 1-2, (e) 1-3. Blue: $V = 100\gamma_\uparrow$, $\Delta\omega = \gamma_\uparrow$; red: $V = 5\gamma_\uparrow$, $\Delta\omega = \gamma_\uparrow$, green: $V = 20\gamma_\uparrow$, $\Delta\omega = 20\gamma_\uparrow$; $\omega_1 = 8\pi$, $\gamma_\uparrow = 0.01$, $\theta = 0$.

As seen in fig. 3.6, all three systems show low values for $|C_\psi|$ when weakly coupled and high values when

strongly coupled. In the systems consisting of three oscillators however this divide is more significant, especially for the chain coupled system. The increased gap makes sense because the Arnold tongues for three oscillators, with chain coupling in particular, are smaller than those for the two oscillator system. This is further supported by the slight shift to the left of the distribution for the strongly coupled system in (d) and (e). The shift is most prominently shown in (e) since $\Delta\omega_{3,1} = \Delta\omega_{2,1} + \Delta\omega_{3,2} = 2\Delta\omega$ and with chain coupling the oscillators are even indirectly coupled. The green bars, valid for a system in a region with poor synchronisation outside the Arnold tongue, through $|C_\psi|$ appears to show a decent amount of synchronisation. However here $|C_\psi|$ like previously mentioned is increased by trajectories without synchronisation, as becomes clear when looking at the other indicators.

3.4.2 $\Delta\phi_\psi$ distributions

Next the distributions of the phase difference $\Delta\phi_\psi$ are shown and discussed:

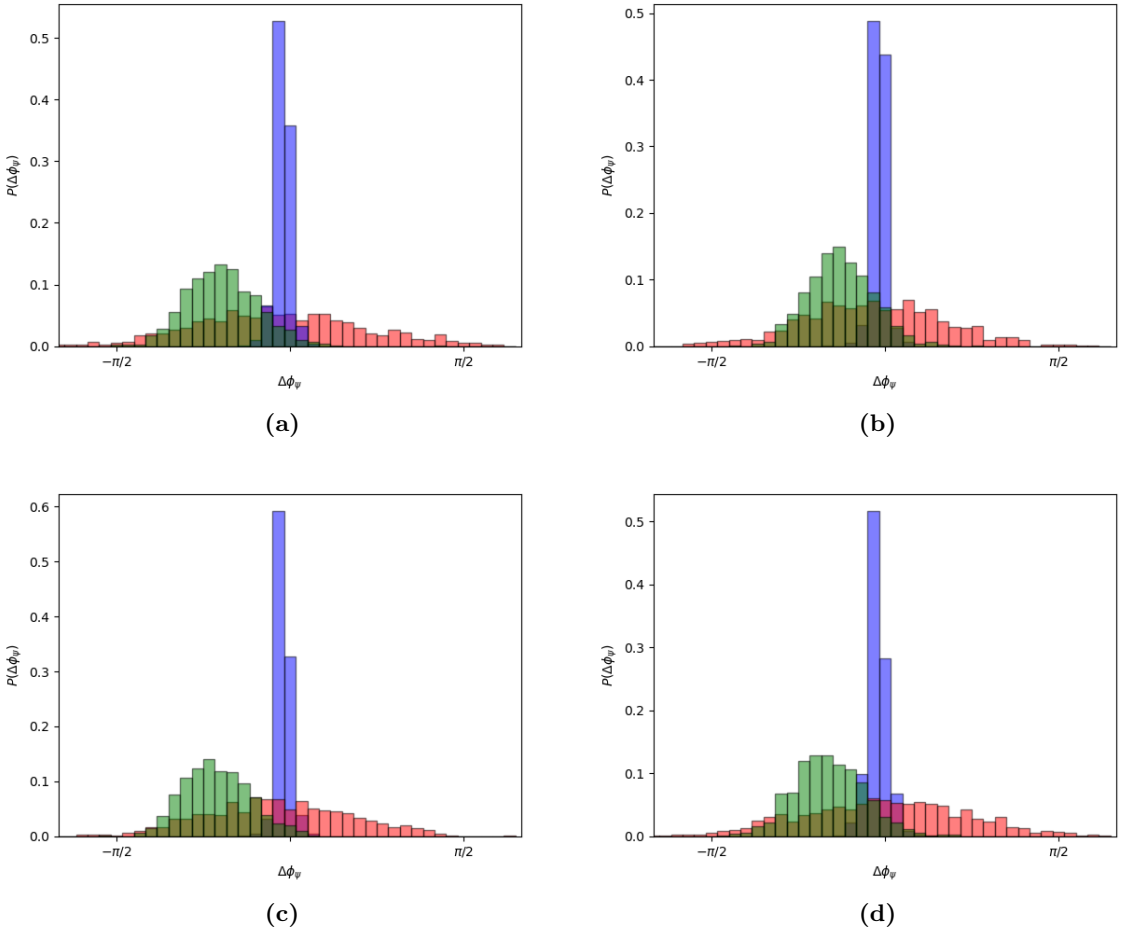

(a) **(b)**

(c) **(d)**

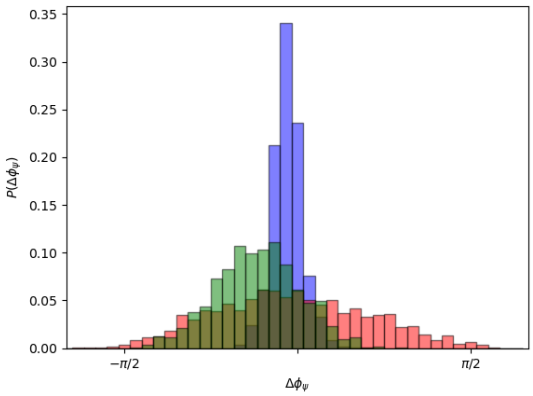

(e)

Fig. 3.7: Probability distribution of $\Delta\phi_\psi$ for different oscillator pairs. 2QVdPOs: (a); 3 all-to-all coupled QVdPOs: (b) 1-2, (c) 1-3; 3 chain coupled QVdPOs: (d) 1-2, (e) 1-3. Blue: $V = 100\gamma_\uparrow$, $\Delta\omega = \gamma_\uparrow$; red: $V = 5\gamma_\uparrow$, $\Delta\omega = \gamma_\uparrow$, green: $V = 20\gamma_\uparrow$, $\Delta\omega = 20\gamma_\uparrow$; $\omega_1 = 8\pi$, $\gamma_\uparrow = 0.01$, $\theta = 0$.

The distributions in fig. 3.7 support the notion of synchronisation in the strongly coupled regime, as the blue histograms are sharply peaked around zero, but the red and green distributions remain a lot broader. Again the systems with a wider Arnold tongue show a somewhat sharper peak. For the case with poor synchronisation outside the Arnold tongue $\Delta\phi_\psi$ is not centred around zero, indicating that synchronisation with the angle $\theta = 0$ is not achieved.

3.4.3 *r* distributions

Here we present the distributions for the Pearson correlator, r, which like $|C_\psi|$ also gives the strength of synchronisation in the system:

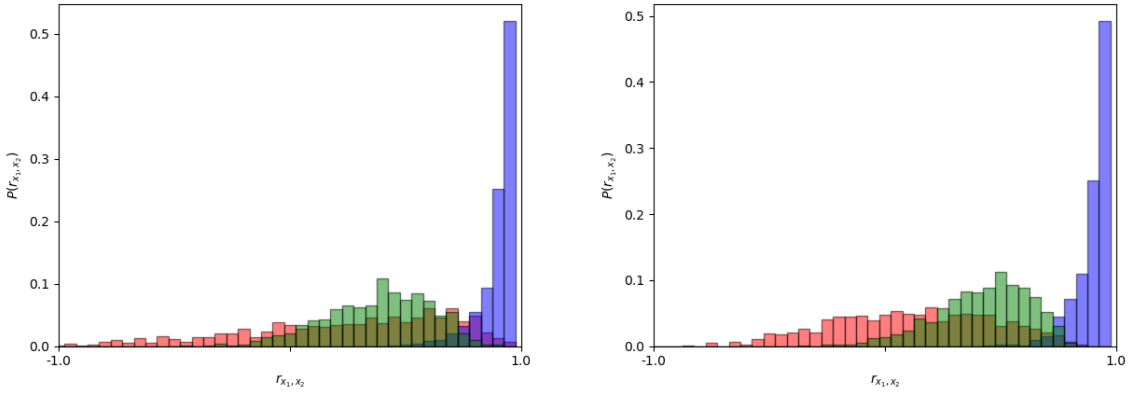

(a) **(b)**

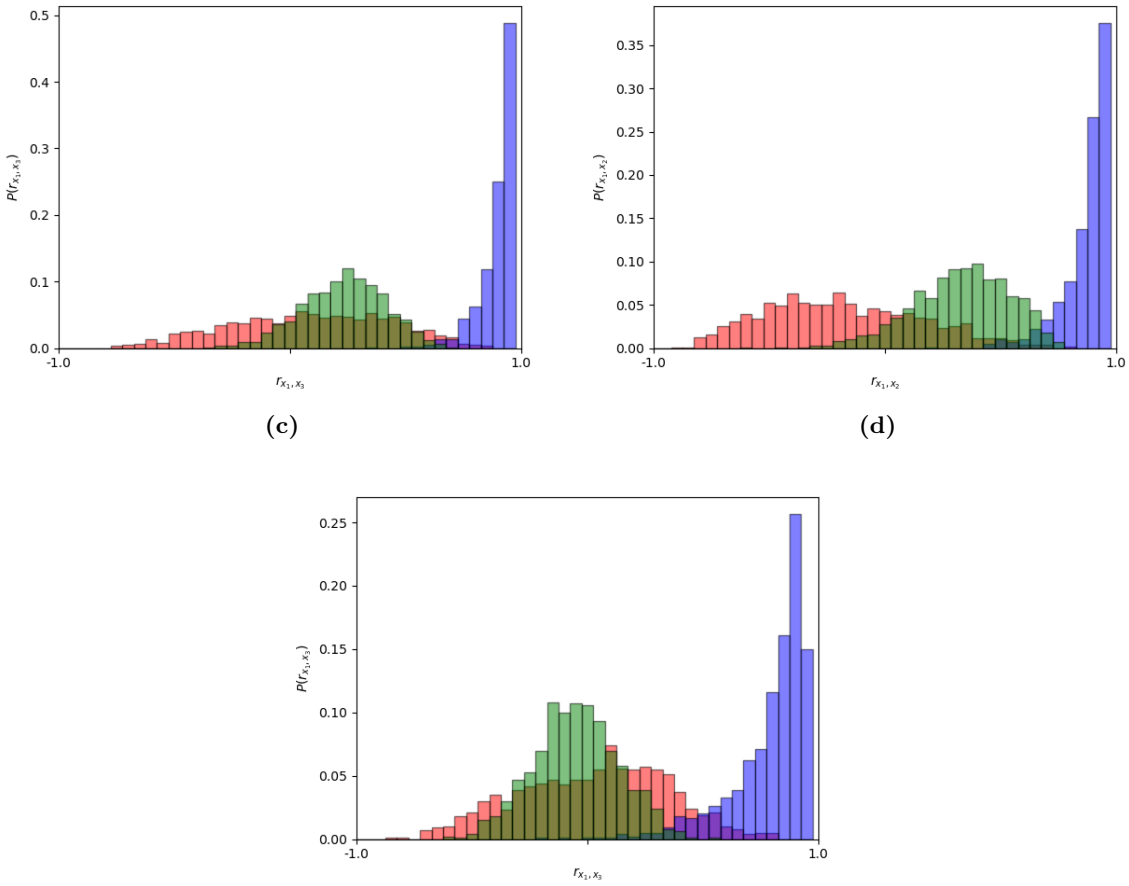

(c) **(d)**

(e)

Fig. 3.8: Probability distribution of r_{x_i,x_j} for different oscillator pairs. 2QVdPOs: (a); 3 all-to-all coupled QVdPOs: (b) 1-2, (c) 1-3; 3 chain coupled QVdPOs: (d) 1-2, (e) 1-3. Blue: $V = 100\gamma_\uparrow$, $\Delta\omega = \gamma_\uparrow$; red: $V = 5\gamma_\uparrow$, $\Delta\omega = \gamma_\uparrow$, green: $V = 20\gamma_\uparrow$, $\Delta\omega = 20\gamma_\uparrow$; $\omega_1 = 8\pi$, $\gamma_\uparrow = 0.01$, $\theta = 0$.

The Pearson correlator in fig. 3.8 shows results in line with the previous indicators. For strong coupling its value peaks close to 1, indicating positive linear correlation between the oscillators. Within areas of poor synchronisation the distributions are closer to zero, suggesting there is no linear correlation between the oscillators. This manifests itself the most in the 1-3 pair of the chain coupled system, since the difference between the eigenfrequencies of these oscillators is the biggest and they are not directly coupled. The slight shift of the red distribution in (d) towards negative correlation might be explained by the coupling between 1-2 and 2-3 effectively only pulling oscillator 2 out of synchronisation with the only oscillators when oscillators 1 and 3 are not synchronised.

3.4.4 S_ψ distributions

Now we look at results for the Von Neumann entropy, S_ψ, of the systems and discuss the relation between synchronisation and entanglement in them:

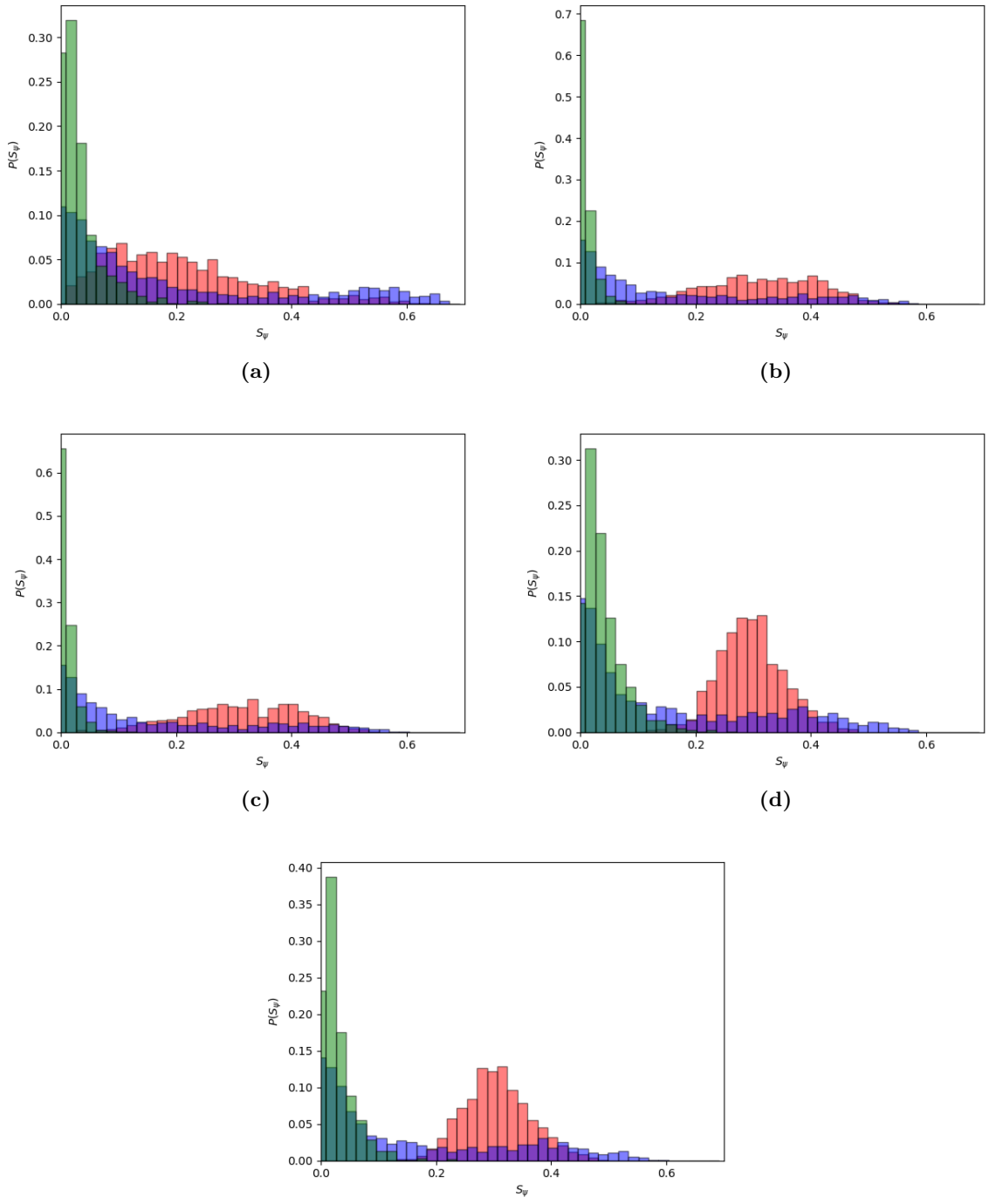

Fig. 3.9: Probability distribution of S_ψ for different oscillator pairs. 2QVdPOs: (a); 3 all-to-all coupled QVdPOs: (b) 1-2, (c) 1-3; 3 chain coupled QVdPOs: (d) 1-2, (e) 1-3. Blue: $V = 100\gamma_\uparrow$, $\Delta\omega = \gamma_\uparrow$; red: $V = 5\gamma_\uparrow$, $\Delta\omega = \gamma_\uparrow$, green: $V = 20\gamma_\uparrow$, $\Delta\omega = 20\gamma_\uparrow$; $\omega_1 = 8\pi$, $\gamma_\uparrow = 0.01$, $\theta = 0$.

Values before associated with strong synchronisation in fig. 3.9 show a larger probability for higher values of S_ψ and thus more entanglement. Less entanglement comes paired with weak synchronisation inside the Arnold tongue as indicated in red. The green distribution shows very little entanglement for the system outside of the synchronisation regime. Differences in the entanglement of systems showing

strong and weak synchronisation, found in two coupled QVdPOs, remain in three oscillator systems even though the highest values for S_ψ are less likely to be reached. It is remarkable how in the three oscillator system, in particular with chain coupling, weakly coupled oscillators show entanglement distributions centred around bigger S_ψ values. An explanation for this can be found in the fact, that due to the extra link in the system, a single oscillator does not only feel the influence of the added oscillator, but also becomes more dependent on the dynamics of the QVdPO that was already present since these start to change more frequently.

4 Conclusion

In this thesis, we have explored the behaviour of all-to-all and chain coupled systems consisting of three quantum Van der Pol oscillators using trajectories. In order to ease the analysis of the quantum system and understand its properties, first similar classical VdPOs were explored. From these CVdPOs, it became clear that the classical systems have a stable limit cycle and within a certain range of parameters, called the Arnold tongue, show synchronisation of the oscillators.
The quantum VdPO was found to be equal to the CVdPO in the classical limit ($\gamma_\downarrow \to 0$). In the quantum limit ($\gamma_\downarrow/\gamma_\uparrow \to \infty$), QVdPOs were shown to have a representation consisting of two spin states. Synchronisation and entanglement in the two-QVdPO system were explored using the methods of [2]. The four indicators used there showed slightly different results for the simulations presented here. Still these results support their conclusions about the occurrence of synchronisation in the trajectories of the system within the quantum Arnold tongue and about the presence of a correlation between this synchronisation and entanglement of the system.
With the same Monte Carlo simulation and indicators, trajectories for three QVdPOs were analysed. The system was expanded to an all-to-all coupled and a chain coupled 3-QVdPO system. Arnold tongues for these systems were found to be smaller and synchronisation occurred slightly less under the same circumstances than within the 2-oscillator system. Entanglement for three weakly coupled oscillators was shown to be a little higher but the positive correlation between synchronisation and strong entanglement remained.

To improve upon the results obtained here for the quantum systems, the Monte Carlo simulation could be adjusted to include a longer period to let trajectories evolve from the initial states used. Averaging indicator values for trajectories over longer time periods would likely also improve the results and might bridge the gap between results shown here and in [2], but both are computationally expensive.
In further works the 3-oscillator structures made in this thesis could be used to build larger networks of oscillators and predict their behaviour. The influence of the strength of the coupling between the three oscillators could also be explored by setting this to different values for different links.

References

[1] K. Rompala, R. Rand, and H. Howland. Dynamics of three coupled van der Pol oscillators with application to circadian rhythms. *Communications in Nonlinear Science and Numerical Simulation*, 12(5):794 – 803, 2007. ISSN 1007-5704. doi: https://doi.org/10.1016/j.cnsns.2005.08.002. URL http://www.sciencedirect.com/science/article/pii/S1007570405001206.

[2] N. Es'haqi-Sani, G. Manzano, R. Zambrini, and R. Fazio. Synchronization along quantum trajectories. *Physical Review Research*, 2(2):23101, 2020. ISSN 2643-1564. doi: 10.1103/physrevresearch.2.023101. URL https://doi.org/10.1103/PhysRevResearch.2.023101.

[3] A. Pikovsky, M. Rosenblum, and J. Kurths. *Synchronization: A Universal Concept in Nonlinear Science*. Cambridge University Press, Cambridge, United Kingdom, 2001. ISBN 13:978-0-521-59285-7.

[4] S.H. Strogatz. *Nonlinear Dynamics and Chaos: With Applications to Physics, Biology, Chemistry and Engeneering, 2nd edition*. CRC Press, Boca Raton, FL, 2018. ISBN 13:978-0-8133-4910-7.

[5] K. Ishibashi and R. Kanamoto. Oscillation collapse in coupled quantum van der Pol oscillators. *Physical Review E*, 96:052210, Nov 2017. doi: 10.1103/PhysRevE.96.052210. URL https://link.aps.org/doi/10.1103/PhysRevE.96.052210.

[6] T.E. Lee and H.R. Sadeghpour. Quantum Synchronization of Quantum van der Pol Oscillators with Trapped Ions. *Physical Review Letters*, 111:234101, Dec 2013. doi: 10.1103/PhysRevLett.111.234101. URL https://link.aps.org/doi/10.1103/PhysRevLett.111.234101.

[7] T.E. Lee, C.K. Chan, and S. Wang. Entanglement tongue and quantum synchronization of disordered oscillators. *Physical Review E*, 89:022913, Feb 2014. doi: 10.1103/PhysRevE.89.022913. URL https://link.aps.org/doi/10.1103/PhysRevE.89.022913.

[8] S. Walter, A. Nunnenkamp, and C. Bruder. Quantum synchronization of two van der pol oscillators. *Annalen der Physik*, 527(1-2):131–138, 2015. doi: https://doi.org/10.1002/andp.201400144. URL https://onlinelibrary.wiley.com/doi/abs/10.1002/andp.201400144.

[9] S. Walter, A. Nunnenkamp, and C. Bruder. Quantum Synchronization of a Driven Self-Sustained Oscillator. *Physical Review Letters*, 112:094102, Mar 2014. doi: 10.1103/PhysRevLett.112.094102. URL https://link.aps.org/doi/10.1103/PhysRevLett.112.094102.

[10] M. Braun. *Differential Equations and Their Applications, 4th edition*. Springer, New York, NY, 1992. ISBN 0-387-97894-1.

[11] J.L. López, S. Abbasbandy, and R. López-Ruiz. Formulas for the amplitude of the van der pol limit cycle through the homotopy analysis method. *Scholary Research Exchange*, 2009, 04 2009. doi: 10.3814/2009/854060. URL https://www.researchgate.net/publication/26620792_Formulas_for_the_Amplitude_of_the_van_der_Pol_Limit_Cycle_through_the_Homotopy_Analysis_Method.

[12] R. Adler. A study of locking phenomena in oscillators. *Proceedings of the IEEE*, 61(10):1380–1385, 1973. doi: 10.1109/PROC.1973.9292.

[13] J.R. Johansson, P.D. Nation, and F. Nori. QuTiP: An open-source Python framework for the dynamics of open quantum systems. *Computer Physics Communications*, 183(8):1760 – 1772, 2012. ISSN 0010-4655. doi: https://doi.org/10.1016/j.cpc.2012.02.021. URL http://www.sciencedirect.com/science/article/pii/S0010465512000835.

[14] Code used producing this thesis. URL https://github.com/Timklijnjan/QVdPOsBEP.git.

A Appendix

Here the connection is shown between the regular and spin representation for the two VdP oscillator system with identical pumping and damping rates in the quantum limit ($\kappa_2 \to \infty$ with $\kappa_1 << \kappa_2$). The regular representation looks like:

$$\begin{aligned}\dot{\rho} =& -i[H,\rho] + \kappa_1 \sum_n (2a_n^\dagger \rho a_n - a_n a_n^\dagger \rho - \rho a_n a_n^\dagger) + \kappa_2 \sum_n (2a_n^2 \rho a_n^{\dagger 2} - a_n^{\dagger 2} a_n^2 \rho - \rho a_n^{\dagger 2} a_n^2) \\ &+ V(2(a_1 - e^{i\theta}a_2)\rho(a_1 - e^{i\theta}a_2)^\dagger - (a_1 - e^{i\theta}a_2)^\dagger(a_1 - e^{i\theta}a_2)\rho - \rho(a_1 - e^{i\theta}a_2)^\dagger(a_1 - e^{i\theta}a_2))\end{aligned} \tag{A.1}$$

Where the Hamiltonian is given by $H = \sum_n \omega_n a_n^\dagger a_n$; the sums with index n account for the individual oscillators; the first sum gives the linear part with rate κ_1; the second the non-linear component with rate κ_2; the systems are coupled with strength V and the coupling is set to a relative phase through the angle θ. To show how in the limit given above this system may be represented using spin operators $\sigma_n^- = |0\rangle\langle 1|_n$ and $\sigma_n^+ = |1\rangle\langle 0|_n$ and Fock states $|0\rangle$, $|1\rangle$ corresponding to $|\downarrow\rangle$ and $|\uparrow\rangle$, we use the following evaluations of the ladder operators:
$a|n\rangle = \sqrt{n}\,|n-1\rangle; \quad \langle n|\,a^\dagger = \langle n-1|\sqrt{n}; \quad a^\dagger|n\rangle = \sqrt{n+1}\,|n+1\rangle; \quad \langle n|\,a = \langle n+1|\sqrt{n+1}.$
First the elements $\langle n_1, n_2|\,\dot{\rho}\,|m_1, m_2\rangle$ are found using these relations and A.1. Since in the quantum limit only the lowest two Fock states, $|0\rangle$ and $|1\rangle$, are occupied due to instantaneous decay of higher states to a lower state, we assume values for states higher than $|2\rangle$ to be zero, for instance $\langle 3,0|\,\rho\,|3,0\rangle \approx 0$. Then the fact that the system relaxes to the steady state very rapidly ($\kappa_2 >> \kappa_1$) is used to set one side of the found equations equal to zero. Coupling terms are omitted during the last step and evaluated separately later on. The equations for the various elements are:

$$\begin{aligned}\langle 0,0|\,\dot{\rho}\,|0,0\rangle =& -4\kappa_1 \langle 0,0|\,\rho\,|0,0\rangle + 4\kappa_2(\langle 2,0|\,\rho\,|2,0\rangle + \langle 0,2|\,\rho\,|0,2\rangle) \\ &+ 2V(\langle 1,0|\,\rho\,|1,0\rangle - e^{-i\theta}\langle 1,0|\,\rho\,|0,1\rangle - e^{i\theta}\langle 0,1|\,\rho\,|1,0\rangle + \langle 0,1|\,\rho\,|0,1\rangle)\end{aligned} \tag{A.2}$$

$$\begin{aligned}\langle 1,0|\,\dot{\rho}\,|1,0\rangle =& \kappa_1(2\langle 0,0|\,\rho\,|0,0\rangle - 6\langle 1,0|\,\rho\,|1,0\rangle) + \kappa_2(4\langle 1,2|\,\rho\,|1,2\rangle + 12\langle 3,0|\,\rho\,|3,0\rangle) \\ &+ V[4\langle 2,0|\,\rho\,|2,0\rangle - 2\sqrt{2}e^{-i\theta}\langle 2,0|\,\rho\,|1,1\rangle + 2\sqrt{2}e^{i\theta}\langle 1,1|\,\rho\,|2,0\rangle + 2\langle 1,1|\,\rho\,|1,1\rangle \\ &- 2\langle 1,0|\,\rho\,|1,0\rangle + e^{-i\theta}\langle 1,0|\,\rho\,|0,1\rangle + e^{i\theta}\langle 0,1|\,\rho\,|1,0\rangle]\end{aligned} \tag{A.3}$$

$$\begin{aligned}\langle 0,1|\,\dot{\rho}\,|0,1\rangle =& \kappa_1(2\langle 0,0|\,\rho\,|0,0\rangle - 6\langle 0,1|\,\rho\,|0,1\rangle) + \kappa_2(4\langle 2,1|\,\rho\,|2,1\rangle + 12\langle 0,3|\,\rho\,|0,3\rangle) \\ &+ V[2\langle 1,1|\,\rho\,|1,1\rangle - 2\sqrt{2}e^{-i\theta}\langle 1,1|\,\rho\,|0,2\rangle + 2\sqrt{2}e^{i\theta}\langle 0,2|\,\rho\,|1,1\rangle + 4\langle 0,2|\,\rho\,|0,2\rangle \\ &- 2\langle 0,1|\,\rho\,|0,1\rangle + e^{-i\theta}\langle 1,0|\,\rho\,|0,1\rangle + e^{i\theta}\langle 0,1|\,\rho\,|1,0\rangle]\end{aligned} \tag{A.4}$$

$$\begin{aligned}\langle 1,1|\,\dot{\rho}\,|1,1\rangle =& \kappa_1(2\langle 0,1|\,\rho\,|0,1\rangle + 2\langle 1,0|\,\rho\,|1,0\rangle - 8\langle 1,1|\,\rho\,|1,1\rangle) \\ &+ V[4\langle 2,1|\,\rho\,|2,1\rangle - 4e^{-i\theta}\langle 2,1|\,\rho\,|1,2\rangle - 4e^{i\theta}\langle 1,2|\,\rho\,|2,1\rangle + 4\langle 1,2|\,\rho\,|1,2\rangle - 4\langle 1,1|\,\rho\,|1,1\rangle \\ &+ \sqrt{2}(e^{i\theta}\langle 0,2|\,\rho\,|1,1\rangle + e^{-i\theta}\langle 2,0|\,\rho\,|1,1\rangle + e^{i\theta}\langle 1,1|\,\rho\,|2,0\rangle + e^{-i\theta}\langle 1,1|\,\rho\,|0,2\rangle)]\end{aligned} \tag{A.5}$$

Now using this and the fact that the system relaxes to the steady state very rapidly ($\kappa_2 >> \kappa_1$) neglecting the coupling for now, setting the left hand sides of A.2, A.3 and A.4 equal to zero we obtain:

$$\langle 2,0|\,\rho\,|2,0\rangle + \langle 0,2|\,\rho\,|0,2\rangle = \frac{\kappa_1}{\kappa_2}\langle 0,0|\,\rho\,|0,0\rangle \tag{A.6}$$

$$\langle 1,0|\,\rho\,|1,0\rangle = \frac{1}{3}\langle 0,0|\,\rho\,|0,0\rangle + \frac{2\kappa_2}{3\kappa_1}\langle 1,2|\,\rho\,|1,2\rangle \tag{A.7}$$

$$\langle 0,1|\,\rho\,|0,1\rangle = \frac{1}{3}\langle 0,0|\,\rho\,|0,0\rangle + \frac{2\kappa_2}{3\kappa_1}\langle 2,1|\,\rho\,|2,1\rangle \tag{A.8}$$

Then following the same procedure for another few states(leaving out higher state terms and coupling except for the first evaluation): Thus:

$$\langle 1,1|\,\rho\,|1,1\rangle = \frac{1}{4}(\langle 1,0|\,\rho\,|1,0\rangle + \langle 0,1|\,\rho\,|0,1\rangle) \tag{A.9}$$

$$\langle 2,1|\,\dot{\rho}\,|2,1\rangle = \kappa_1(4\,\langle 1,1|\,\rho\,|1,1\rangle + 2\,\langle 2,0|\,\rho\,|2,0\rangle - 10\,\langle 2,1|\,\rho\,|2,1\rangle) - 4\kappa_2\,\langle 2,1|\,\rho\,|2,1\rangle \tag{A.10}$$

Giving:

$$\langle 2,1|\,\rho\,|2,1\rangle = \kappa_1\frac{2\,\langle 1,1|\,\rho\,|1,1\rangle + \langle 2,0|\,\rho\,|2,0\rangle}{5\kappa_1 + 2\kappa_2} \tag{A.11}$$

$$\langle 1,2|\,\dot{\rho}\,|1,2\rangle = \kappa_1(4\,\langle 1,1|\,\rho\,|1,1\rangle + 2\,\langle 0,2|\,\rho\,|0,2\rangle - 10\,\langle 1,2|\,\rho\,|1,2\rangle) - 4\kappa_2\,\langle 1,2|\,\rho\,|1,2\rangle \tag{A.12}$$

Therefore:

$$\langle 1,2|\,\rho\,|1,2\rangle = \kappa_1\frac{2\,\langle 1,1|\,\rho\,|1,1\rangle + \langle 0,2|\,\rho\,|0,2\rangle}{5\kappa_1 + 2\kappa_2} \tag{A.13}$$

Substituting A.11, A.13 and finally A.9 after adding A.7 and A.8 gives:

$$\langle 1,0|\,\rho\,|1,0\rangle + \langle 0,1|\,\rho\,|0,1\rangle = \frac{2}{3}\left(\langle 0,0|\,\rho\,|0,0\rangle + \kappa_2\frac{\langle 1,0|\,\rho\,|1,0\rangle + \langle 0,1|\,\rho\,|0,1\rangle + \langle 2,0|\,\rho\,|2,0\rangle + \langle 0,2|\,\rho\,|0,2\rangle}{5\kappa_1 + 2\kappa_2}\right) \tag{A.14}$$

Dividing A.6 by $\frac{\kappa_2}{\kappa_1}$, plugging it into the equation above and rearranging the terms we arrive at:

$$\langle 1,0|\,\rho\,|1,0\rangle + \langle 0,1|\,\rho\,|0,1\rangle = \frac{\kappa_2}{\kappa_1}\frac{12\frac{\kappa_1}{\kappa_2} + 4}{15\frac{\kappa_1}{\kappa_2} + 4}(\langle 2,0|\,\rho\,|2,0\rangle + \langle 0,2|\,\rho\,|0,2\rangle) \tag{A.15}$$

Now we look at the spin representation suggested in [2]:

$$\begin{aligned}\dot{\rho} =& -i[H,\rho] + \kappa_1\sum_n(2\sigma_n^+\rho\sigma_n^- - \sigma_n^-\sigma_n^+\rho - \rho\sigma_n^-\sigma_n^+) + 2\kappa_1\sum_n(2\sigma_n^-\rho\sigma_n^+ - \sigma_n^+\sigma_n^-\rho - \rho\sigma_n^+\sigma_n^-)\\ &+ V(2(\sigma_1^- - e^{i\theta}\sigma_2^-)\rho(\sigma_1^- - e^{i\theta}\sigma_2^-)^\dagger - (\sigma_1^- - e^{i\theta}\sigma_2^-)^\dagger(\sigma_1^- - e^{i\theta}\sigma_2^-)\rho - \rho(\sigma_1^- - e^{i\theta}\sigma_2^-)^\dagger(\sigma_1^- - e^{i\theta}\sigma_2^-))\end{aligned} \tag{A.16}$$

Disregarding the coupling for the ground state we have:

$$\langle 0,0|\,\dot{\rho}\,|0,0\rangle = -4\kappa_1\,\langle 0,0|\,\rho\,|0,0\rangle + 4\kappa_1(\langle 1,0|\,\rho\,|1,0\rangle + \langle 0,1|\,\rho\,|0,1\rangle) \tag{A.17}$$

To see how this compares to A.2 we substitute A.15 into the equation above:

$$\langle 0,0|\,\dot{\rho}\,|0,0\rangle = -4\kappa_1\,\langle 0,0|\,\rho\,|0,0\rangle + 4\kappa_2\frac{12\frac{\kappa_1}{\kappa_2} + 4}{15\frac{\kappa_1}{\kappa_2} + 4}(\langle 2,0|\,\rho\,|2,0\rangle + \langle 0,2|\,\rho\,|0,2\rangle) \tag{A.18}$$

Where $\frac{\kappa_1}{\kappa_2} \to 0$ as the limit of $\frac{\kappa_2}{\kappa_1} \to \infty$ was assumed thus giving equal evaluations for the regular and spin representation of the system. Next we look at the coupling term of A.16:

$$\langle 0,0|\,\dot{\rho}\,|0,0\rangle = 2V(\langle 1,0|\,\rho\,|1,0\rangle - e^{-i\theta}\,\langle 1,0|\,\rho\,|0,1\rangle - e^{i\theta}\,\langle 0,1|\,\rho\,|1,0\rangle + \langle 0,1|\,\rho\,|0,1\rangle) \tag{A.19}$$

The above is exactly the evaluation found for A.1. The comparison should also hold for states with Fock state $|1\rangle$, from A.16 we obtain:

$$\langle 1,1|\,\dot{\rho}\,|1,1\rangle = \kappa_1(2\,\langle 0,1|\,\rho\,|0,1\rangle + 2\,\langle 1,0|\,\rho\,|1,0\rangle - 8\,\langle 1,1|\,\rho\,|1,1\rangle) - 4V\,\langle 1,1|\,\rho\,|1,1\rangle \tag{A.20}$$

$$\begin{aligned}\langle 1,0|\,\dot{\rho}\,|1,0\rangle =& \kappa_1(2\,\langle 0,0|\,\rho\,|0,0\rangle - 6\,\langle 1,0|\,\rho\,|1,0\rangle + 4\,\langle 1,1|\,\rho\,|1,1\rangle)\\ &+ V(2\,\langle 1,1|\,\rho\,|1,1\rangle - 2\,\langle 1,0|\,\rho\,|1,0\rangle + e^{i\theta}\,\langle 0,1|\,\rho\,|1,0\rangle + e^{-i\theta}\,\langle 1,0|\,\rho\,|0,1\rangle)\end{aligned} \tag{A.21}$$

$$\begin{aligned}\langle 0,1|\,\dot{\rho}\,|0,1\rangle =& \kappa_1(2\,\langle 0,0|\,\rho\,|0,0\rangle - 6\,\langle 0,1|\,\rho\,|0,1\rangle + 4\,\langle 1,1|\,\rho\,|1,1\rangle)\\ &+ V(2\,\langle 1,1|\,\rho\,|1,1\rangle - 2\,\langle 0,1|\,\rho\,|0,1\rangle + e^{i\theta}\,\langle 0,1|\,\rho\,|1,0\rangle + e^{-i\theta}\,\langle 1,0|\,\rho\,|0,1\rangle)\end{aligned} \tag{A.22}$$

To see the resemblance with the evaluations of the original representation we use that representation to evaluate a few more states:

$$\langle 2,0|\,\dot{\rho}\,|1,1\rangle = -i(\omega_1-\omega_2)\,\langle 2,0|\,\rho\,|1,1\rangle + \kappa_1(2\sqrt{2}\,\langle 1,0|\,\rho\,|0,1\rangle - 8\,\langle 2,0|\,\rho\,|1,1\rangle) - 2\kappa_2\,\langle 2,0|\,\rho\,|1,1\rangle \tag{A.23}$$

From which we get:

$$\langle 2,0|\,\rho\,|1,1\rangle = \frac{\kappa_1 2\sqrt{2}}{i(\omega_1-\omega_2) + 8\kappa_1 + 2\kappa_2}\,\langle 1,0|\,\rho\,|0,1\rangle \tag{A.24}$$

Likewise:

$$\langle 1,1|\,\dot{\rho}\,|2,0\rangle = -i(\omega_2-\omega_1)\,\langle 1,1|\,\rho\,|2,0\rangle + \kappa_1(2\sqrt{2}\,\langle 0,1|\,\rho\,|1,0\rangle - 8\,\langle 1,1|\,\rho\,|2,0\rangle) - 2\kappa_2\,\langle 1,1|\,\rho\,|2,0\rangle \quad \text{(A.25)}$$

leads to:

$$\langle 1,1|\,\rho\,|2,0\rangle = \frac{\kappa_1 2\sqrt{2}}{i(\omega_2-\omega_1)+8\kappa_1+2\kappa_2}\,\langle 0,1|\,\rho\,|1,0\rangle \quad \text{(A.26)}$$

$$\langle 0,2|\,\dot{\rho}\,|1,1\rangle = -i(\omega_2-\omega_1)\,\langle 0,2|\,\rho\,|1,1\rangle + \kappa_1(2\sqrt{2}\,\langle 0,1|\,\rho\,|1,0\rangle - 8\,\langle 0,2|\,\rho\,|1,1\rangle) - 2\kappa_2\,\langle 0,2|\,\rho\,|1,1\rangle \quad \text{(A.27)}$$

to:

$$\langle 0,2|\,\rho\,|1,1\rangle = \frac{\kappa_1 2\sqrt{2}}{i(\omega_2-\omega_1)+8\kappa_1+2\kappa_2}\,\langle 0,1|\,\rho\,|1,0\rangle \quad \text{(A.28)}$$

And:

$$\langle 1,1|\,\dot{\rho}\,|0,2\rangle = -i(\omega_1-\omega_2)\,\langle 1,1|\,\rho\,|0,2\rangle + \kappa_1(2\sqrt{2}\,\langle 1,0|\,\rho\,|0,1\rangle - 8\,\langle 1,1|\,\rho\,|0,2\rangle) - 2\kappa_2\,\langle 1,1|\,\rho\,|0,2\rangle \quad \text{(A.29)}$$

to:

$$\langle 1,1|\,\rho\,|0,2\rangle = \frac{\kappa_1 2\sqrt{2}}{i(\omega_1-\omega_2)+8\kappa_1+2\kappa_2}\,\langle 1,0|\,\rho\,|0,1\rangle \quad \text{(A.30)}$$

Now since:

$$\langle 1,0|\,\dot{\rho}\,|0,1\rangle = -i(\omega_1-\omega_2)\,\langle 1,0|\,\rho\,|0,1\rangle + -6\kappa_1\,\langle 1,0|\,\rho\,|0,1\rangle \quad \text{(A.31)}$$

and:

$$\langle 0,1|\,\dot{\rho}\,|1,0\rangle = -i(\omega_2-\omega_1)\,\langle 0,1|\,\rho\,|1,0\rangle + -6\kappa_1\,\langle 0,1|\,\rho\,|1,0\rangle \quad \text{(A.32)}$$

result in:

$$\langle 0,1|\,\rho\,|1,0\rangle = \langle 1,0|\,\rho\,|0,1\rangle = 0 \quad \text{(A.33)}$$

A.24,A.26, A.28 and A.30 also equal zero. This in turn combined with:

$$\langle 2,1|\,\dot{\rho}\,|1,2\rangle = -i(\omega_1-\omega_2)\,\langle 2,1|\,\rho\,|1,2\rangle + \kappa_1(2\sqrt{2}\,\langle 1,1|\,\rho\,|0,2\rangle + 2\sqrt{2}\,\langle 2,0|\,\rho\,|1,1\rangle - 10\,\langle 2,1|\,\rho\,|1,2\rangle) \quad \text{(A.34)}$$

and:

$$\langle 1,2|\,\dot{\rho}\,|2,1\rangle = -i(\omega_2-\omega_1)\,\langle 2,1|\,\rho\,|1,2\rangle + \kappa_1(2\sqrt{2}\,\langle 0,2|\,\rho\,|1,1\rangle + 2\sqrt{2}\,\langle 1,1|\,\rho\,|2,0\rangle - 10\,\langle 1,2|\,\rho\,|2,1\rangle) \quad \text{(A.35)}$$

gives:

$$\langle 2,1|\,\rho\,|1,2\rangle = \langle 1,2|\,\rho\,|2,1\rangle = 0 \quad \text{(A.36)}$$

The realisation that:

$$\begin{aligned}\langle 2,1|\,\rho\,|2,1\rangle + \langle 1,2|\,\rho\,|1,2\rangle &= \kappa_1\frac{4\,\langle 1,1|\,\rho\,|1,1\rangle + \langle 2,0|\,\rho\,|2,0\rangle + \langle 2,0|\,\rho\,|2,0\rangle}{5\kappa_1+2\kappa_2} \\ &= \frac{\kappa_1}{\kappa_2}\frac{4\,\langle 1,1|\,\rho\,|1,1\rangle + \langle 2,0|\,\rho\,|2,0\rangle + \langle 2,0|\,\rho\,|2,0\rangle}{5\frac{\kappa_1}{\kappa_2}+2}\end{aligned} \quad \text{(A.37)}$$

in the quantum limit equals zero offers te final piece to unify A.5 with A.20 We also obtain:

$$\langle 2,2|\,\dot{\rho}\,|2,2\rangle = \kappa_1(4\,\langle 1,2|\,\rho\,|1,2\rangle - 12\,\langle 2,2|\,\rho\,|2,2\rangle + 4\,\langle 2,1|\,\rho\,|2,1\rangle) - 8\kappa_2\,\langle 2,2|\,\rho\,|2,2\rangle \quad \text{(A.38)}$$

From which follows:

$$\langle 2,2|\,\rho\,|2,2\rangle = \kappa_1\frac{\langle 1,2|\,\rho\,|1,2\rangle + \langle 2,1|\,\rho\,|2,1\rangle}{3\kappa_1+2\kappa_2} \quad \text{(A.39)}$$

So likewise:

$$\begin{aligned}\langle 2,0|\,\rho\,|2,0\rangle &= \frac{\kappa_1\,\langle 1,0|\,\rho\,|1,0\rangle + \kappa_2\,\langle 2,2|\,\rho\,|2,2\rangle}{2\kappa_1+\kappa_2} \\ &= \frac{\kappa_1\,\langle 1,0|\,\rho\,|1,0\rangle}{2\kappa_1+\kappa_2} + \kappa_1\kappa_2\frac{\langle 1,2|\,\rho\,|1,2\rangle + \langle 2,1|\,\rho\,|2,1\rangle}{12\kappa_1^2+14\kappa_1\kappa_2+4\kappa_2^2} \\ &= \frac{\frac{\kappa_1}{\kappa_2}\,\langle 1,0|\,\rho\,|1,0\rangle}{2\frac{\kappa_1}{\kappa_2}+1} + \frac{\kappa_1}{\kappa_2}\frac{\langle 1,2|\,\rho\,|1,2\rangle + \langle 2,1|\,\rho\,|2,1\rangle}{12\frac{\kappa_1^2}{\kappa_2^2}+14\frac{\kappa_1}{\kappa_2}+4}\end{aligned} \quad \text{(A.40)}$$

and

$$\begin{aligned}\langle 0,2|\,\rho\,|0,2\rangle &= \frac{\kappa_1\langle 0,1|\,\rho\,|0,1\rangle + \kappa_2\langle 2,2|\,\rho\,|2,2\rangle}{2\kappa_1+\kappa_2}\\ &= \frac{\kappa_1\langle 0,1|\,\rho\,|0,1\rangle}{2\kappa_1+\kappa_2} + \kappa_1\kappa_2\frac{\langle 1,2|\,\rho\,|1,2\rangle + \langle 2,1|\,\rho\,|2,1\rangle}{12\kappa_1^2+14\kappa_1\kappa_2+4\kappa_2^2}\\ &= \frac{\frac{\kappa_1}{\kappa_2}\langle 0,1|\,\rho\,|0,1\rangle}{2\frac{\kappa_1}{\kappa_2}+1} + \frac{\kappa_1}{\kappa_2}\frac{\langle 1,2|\,\rho\,|1,2\rangle + \langle 2,1|\,\rho\,|2,1\rangle}{12\frac{\kappa_1^2}{\kappa_2^2}+14\frac{\kappa_1}{\kappa_2}+4}\end{aligned} \tag{A.41}$$

reduce to zero in the limit. For A.3 to be equal to A.21 and A.4 to be equal to A.22 we are left with the task to prove in the quantum limit:

$$\kappa_2\langle 1,2|\,\rho\,|1,2\rangle = \kappa_1\langle 1,1|\,\rho\,|1,1\rangle \tag{A.42}$$

and

$$\kappa_2\langle 2,1|\,\rho\,|2,1\rangle = \kappa_1\langle 1,1|\,\rho\,|1,1\rangle \tag{A.43}$$

The first of which follows from:

$$\begin{aligned}\kappa_2\langle 1,2|\,\rho\,|1,2\rangle &= \kappa_1\kappa_2\frac{2\langle 1,1|\,\rho\,|1,1\rangle + \langle 0,2|\,\rho\,|0,2\rangle}{5\kappa_1+2\kappa_2}\\ &= \kappa_1\frac{2\langle 1,1|\,\rho\,|1,1\rangle}{5\frac{\kappa_1}{\kappa_2}+2} + \frac{\kappa_1^2}{\kappa_2}\frac{1}{5\frac{\kappa_1}{\kappa_2}+2}\left(\frac{\langle 0,1|\,\rho\,|0,1\rangle}{2\frac{\kappa_1}{\kappa_2}+1} + \frac{\langle 1,2|\,\rho\,|1,2\rangle + \langle 2,1|\,\rho\,|2,1\rangle}{12\frac{\kappa_1^2}{\kappa_2^2}+14\frac{\kappa_1}{\kappa_2}+4}\right)\end{aligned} \tag{A.44}$$

And in a similar way the second from:

$$\kappa_2\langle 1,2|\,\rho\,|1,2\rangle = \kappa_1\frac{2\langle 1,1|\,\rho\,|1,1\rangle}{5\frac{\kappa_1}{\kappa_2}+2} + \frac{\kappa_1^2}{\kappa_2}\frac{1}{5\frac{\kappa_1}{\kappa_2}+2}\left(\frac{\langle 1,0|\,\rho\,|1,0\rangle}{2\frac{\kappa_1}{\kappa_2}+1} + \frac{\langle 1,2|\,\rho\,|1,2\rangle + \langle 2,1|\,\rho\,|2,1\rangle}{12\frac{\kappa_1^2}{\kappa_2^2}+14\frac{\kappa_1}{\kappa_2}+4}\right) \tag{A.45}$$

All the above taken together thus gives equality of the regular and spin representation in the quantum limit where only two Fock states survive.